Fault Monitoring in Hydraulic Systems using Unscented Kalman Filter

By

Mohammad Sepasi

B.Sc., Sharif University of Technology, Iran, 2005

A THESIS SUBMITTED IN PARTIAL FULFILLMENT
OF THE REQUIREMENTS FOR THE DEGREE OF

MASTER OF APPLIED SCIENCE

in

THE FACULTY OF GRADUATE STUDIES

(Mechanical Engineering)

The University of British Columbia

November 2007

Abstract

Condition monitoring of hydraulic systems is an area that has grown substantially in the last few decades. This thesis presents a scheme that automatically generates the fault symptoms by on-line processing of raw sensor data from a real test rig. The main purposes of implementing condition monitoring in hydraulic systems are to increase productivity, decrease maintenance costs and increase safety. Since such systems are widely used in industry and becoming more complex in function, reliability of the systems must be supported by an efficient monitoring and maintenance scheme.

This work proposes an accurate state space model together with a novel model-based fault diagnosis methodology. The test rig has been fabricated in the Process Automation and Robotics Laboratory at UBC. First, a state space model of the system is derived. The parameters of the model are obtained through either experiments or direct measurements and manufacturer specifications. To validate the model, the simulated and measured states are compared. The results show that under normal operating conditions the simulation program and real system produce similar state trajectories.

For the validated model, a condition monitoring scheme based on the Unscented Kalman Filter (UKF) is developed. In simulations, both measurement and process noises are considered. The results show that the algorithm estimates the

system states with acceptable residual errors. Therefore, the structure is verified to be employed as the fault diagnosis scheme.

Five types of faults are investigated in this thesis: loss of load, dynamic friction load, the internal leakage between the two hydraulic cylinder chambers, and the external leakage at either side of the actuator. Also, for each leakage scenario, three levels of leakage are investigated in the tests. The developed UKF-based fault monitoring scheme is tested on the practical system while different fault scenarios are singly introduced to the system. A sinusoidal reference signal is used for the actuator displacement. To diagnose the occurred fault in real time, three criteria, namely residual moving average of the errors, chamber pressures, and actuator characteristics, are considered. Based on the presented experimental results and discussions, the proposed scheme can accurately diagnose the occurred faults.

CONTENTS

List of Tables

List of Figures

Acknowledgments

I would like to express my deepest appreciation to my advisor, Dr. Farrokh Sassani, for his inspiration, friendship, encouragement, patience and unconditional support. I am extremely fortunate for having the opportunity to work with him and having the freedom to explore science in his laboratory. I am really thankful for his support over the last two years.

I am indebted to Dr. Yusuf Altintas for sharing his lab equipment and Dr. Ryozo Nagamune for being generous with his time and knowledge and providing intellectual support and invaluable comments.

I would like to convey my gratitude to our kind graduate secretary of Mechanical Engineering Department, Ms. Yuki Matsumura. In addition, I would like to extend my sincere thanks to Mr. Glenn Jolly, Mr. Gord Wright, and Mr. Sean Buxton for their essential technical assistance during this research. Additionally, I would like to thank Mr. Perry Yabuno for timely acquisition of electro-mechanical devices required for the fabrication of the set-up. .

I am grateful to my dear colleagues in Process Automation and Robotics Laboratory: Dr. Mohammad Mallakzadeh and Mr. Amin Karami. Their friendship and support made the lab a motivating environment during the period of my work.
I am so lucky to have such supportive friends: Hamidreza Yamini, Vahid Bazargan, and Pirooz Darabi.

Lastly, I wish to express my genuine gratitude to my wonderful family for their never-ending love, support, and guidance. My father's perfectionism and seek

for the truth and my mother's energy, encouragement and moral support have always been a great motivation for me. I also thank my brother, my durable source of inspiration, for his support in every step of my life.

Dedication

To my parents

as an inadequate but sincere expression of appreciation and love

CHAPTER 1

Introduction

1.1 Preliminary Remarks

The advent of hydraulic systems with their speed and reliable force accelerated a rapid development in the modern industry such as heavy-duty industrial robots, mining, material handling and press, manufacturing and construction. Hydraulic systems developed and accompanied by automatic controls allow flexibility in various types of operations, and significantly speed up the processes involved.

Employing hydraulic systems rather than other power transmission systems (e.g., electrical motor) provides a number of relatively important advantages, some of which are the following ([1] Section 4.4 and [2] Chapter 1):

1. Hydraulic fluids carry away heat generated from moving parts in the systems, as well as they act as superb lubricants.
2. Hydraulic actuators can be employed in random and periodic operations without any considerable suffering.

3. Hydraulic actuators can apply large forces with high load stiffness.
4. Load effects are insignificant in hydraulic systems, compared with those in other power transmission systems.
5. Hydraulic systems have long operating lives even if employed in harsh environments.
6. Hydraulic systems have considerably less weight/ power ratio.

However, there are a number of disadvantages associated with hydraulic power systems ([1] Section 4.4 and [2] Chapter 1):

1. Generating hydraulic power is not so readily achievable as is with other forms of powers, e.g. electrical, and mechanical.
2. Hydraulic systems are relatively expensive.
3. Fire and explosion hazards exist during operation.
4. Hydraulic power transmissions produce significant amount of loud noise.
5. Hydraulic system designers face several complex characteristics such as non-linearity.

Wide industrial applications, along with the design challenges, make hydraulic systems one of the most interesting topics in engineering research [3-5].

The main objective of this thesis is to analyze and select the best modeling approach, compromising between model accuracy and model complexity regarding real-time applications and response effectiveness followed by developing, verifying and

integrating modules for the purpose of online monitoring and diagnosis of faults in hydraulic power systems .

In the process engineering and mechanical machinery, diagnosing the occurred faults in the system is an essential issue. Undoubtedly, in some applications such as airplane power systems, faults should be detected and recovered immediately while the plant is still operating to prevent catastrophic system failure and loss of human lives. Fault diagnosis in some other applications, such as off-highway machinery or manufacturing, may not be as critical but nevertheless early diagnosis of plant faults helps enhance the productivity and avoid fault progression leading almost certainly to plant failure. Thereby, there has been considerable interest in this field from practitioners as well as researchers for a number of decades. Based on physical redundancy and analytical redundancy ideas, a wide variety of methodologies have been developed to improve the fault diagnosis in dynamic systems [6]. In the first approach, redundant sensors and actuators are installed in the systems; therefore in the event of a failure, these surplus devices are employed instead of the faulty one. The analytical redundancy approach is founded on the accurate model of the dynamic system. If a malfunction occurs, the difference between the real plant and model behavior will evolve. Once this difference exceeds a set threshold value, it is concluded that the system operates undesirably and tends to function in uncontrollable regions.

1.2 Hydraulic Power Systems

A servo-system is a feedback system consisting of at least the following three essential elements; sensor, servomotor, and controller. As for hydraulic systems, the vast majority of these types of power systems in industrial applications are servo-systems. Beside the mentioned elements, a number of hydraulic components are interconnected to form a practical hydraulic servo-system that provides the desired operational characteristics. The descriptions of fundamental components of a hydraulic servo-system are the following:

Actuator

A Hydraulic actuator (cylinder) employed in a hydraulic system is the motor side of the system as opposed to a pump, which is the generator or driver side of the system. Hydraulic actuators are activated by hydraulic pressure. They transform the fluid's energy to a linear work, which can be either rotational or translational. The actuator comprises a cylinder tube, in which a piston connected to a rod slides. The rod slides out of the cylinder through seals from either one or both sides. The piston, which consists of the sliding rings and seals, divides the inside of the cylinder into two chambers. If the effective areas of both chambers are identical, the cylinder is called symmetric, otherwise it is asymmetric. By pumping hydraulic oil to one side of the hydraulic cylinder, the rod begins sliding toward the other. Hence, the oil is pushed back through the return line to the reservoir from the other chamber.

Pump

The pump is the heart of the hydraulic power system and, as such, is fundamental for an efficient system operation. Typically, the pump supplies the hydraulic power of the system, which is essential to activate the actuator. Most of the hydraulic pumps used in power systems are positive displacement pumps. Positive displacement means that the flow is directly proportional to the speed of the pump. Regarding the internal pump volume, two types of pumps are designated: fixed displacement and variable (adjustable) displacement. Depending on the required pressure and flow, as well as the efficiency and life expectancy, either fixed displacement pump (low budget) or variable displacement pump (high quality) may be chosen. Fixed displacement pumps derive a constant amount of fluid in each revolution of the rotor. To achieve the desired characteristics from hydraulic power system, several kinds of pumps have been developed (e.g., screw pumps, gear pumps, gerotor pumps, vane pumps, and piston pumps).

Servo valve

Servo valves are employed in hydraulic systems to manage the flow of the fluid in the hydraulic circuit pipelines. They, along with the feedback controllers, generate continuously regulated outputs as functions of the electrical inputs. Commonly, the feedback signal is produced by the comparison between the position, velocity, or force of the actuator (end-effector) and reference signal sent to the control valve. Servo valves are designed in single-stage, two-stage, and three-stage models. The single-stage servo-valve, the simplest and least cost, consists of a spool valve whose position is controlled by a torque motor via a direct connection. Multi-stage servo-valves intensify the applied torque of the torque motor using one or two hydraulic amplifiers. Thereby, multi-stage

servo-valves can be employed for higher flow rates and pressures, as well as, they can overcome high friction.

Other components

In addition to the above, several other components are required to complete a hydraulic system, e.g. sensors and pipelines. Sensors must be installed in the proper locations to measure the demanded data; on the contrary, the measurand should not be affected. The feedback controller may need this data to generate the input signal to servo-valve.

Several valves, such as needle valves, pressure relief valves, check valves, are employed to control the pressure, rate of flow, and direction of fluid inside of the circuit. As an instance, the pressure relief valve reduces and controls the pressure not to exceed a certain level. To do so, it connects the high pressure flow to the reservoir. Mostly, the common usage is in the protection of a hydraulic element from the unwanted high pressure.

Generally, a hydraulic circuit is a closed-loop system including a tank as a fluid reservoir. A pump is always necessary to pressurize the fluid, which ordinarily is hydraulic oil. Meanwhile, a servo-valve regulates this high pressure fluid to control the behavior of the end-effector, which could follow a complex trajectory with a required force. For this sake, a controller should be developed. For instance, Dutton and Groves [7] developed an adaptive controller based on a pole-placement algorithm.

Thus far, primary structure of a hydraulic system has been explained. Moreover, regarding a sophisticated hydraulic system, the couplings or interactions emerge from the

existence of signal connections or common elements between the different lines in the circuit [8].

1.3 Potential faults in hydraulic systems

In hydraulic systems, a wide range of faults and failures may occur, which have been extensively investigated by researchers. Chen and Saif [9] developed an iterative learning observer (ILO) for estimation, fault detection and compensation. Their proposed methodology can diagnose multiple faults. Three most common faults in industrial hydraulic systems are fluid contamination [10], supply pressure malfunction [11], and leakage [12].

Heron and Huges [13] developed a novel contaminant monitoring scheme to examine the cleanliness level of fluid in a hydraulic system. Fine solid contaminant emanating from the moving parts in the hydraulic circuit accumulates around the small clearances of spool valves. Consequently, the friction in the valve increases and the system operates erratically. To simulate this fault in their study, the oil was added with various level of contaminants and was passed through the hydraulic system and finally through the contaminant monitor.

Leakages whose effects include a reduced pressure, degraded stability, and decreased efficiency are the most common faults occurring in the practical hydraulic power systems. Leakages are classified into two categories: external and internal. The greatest concern among the related topics is the leakage in Pumps and actuators as they are two essential components in all hydraulic power systems as well as they both contain moving parts accelerating the wear.

Actuator external leakages mostly occur at the location of the connecting hoses and the cylinder. An and Sepehri [14] modeled the external leakages through two bleed valves, each mounted on a bypass to each side of a cylinder. The amount of leakages was tuned by opening these bleed valves. However, they did not quantify the leakage. In 2006, An and Sepehri [15] developed a sequential analysis (SA) and addressed a quantification scheme. The importance of this scheme is in recognizing the progression of the leakage fault. Crowther et al. [12] built a neural network model for a hydraulic actuation system in which the lack of supply pressure, internal leakage in the actuator, and dynamic friction load were investigated. The actuator internal leakage was modeled by a cross-line bleed valve. The internal leakage, which is relatively more common in practice rather than the external one, arises as a consequence of superfluous clearance between the inner wall of the cylinder and the piston. The seal may wear after being in operation for a while. Both types of leakages lead to the demand of higher flow and pressure supply for the recovery intention.

Furthermore, leakage in the hydraulic pump is another aspect of leakage faults. Leakage faults regularly lead to decrease in both the flow rate and pressure in discharge ports. It may happen by virtue of Excessive wear of pump internal clearances or poor sealing. Skormin and Apone [16] developed a failure prediction procedure, detecting and utilizing trends exhibited by parameter estimation. The investigated faults included the leakage of the hydraulic pumps. In addition, there are several minor reasons causing this decline in pressure and flow rate. Two most common of them are a) a pipe, impeller, or suction strainer that may be blocked, and b) The characteristics of the liquid may vary

from the manufacturer specifications, as examples, higher viscosity, or density than expected.

Despite major development, researchers are constantly working on more accurate and fast algorithms, which are suitable for real time applications and more complex systems.

1.4 Research Objectives

As a consequence of all above, over time, operational problems or faults due to factors such as wear, misuse and lack of proper maintenance develop in hydraulic systems. Such trends if not prevented can lead to catastrophic failure. It is therefore, desirable to quickly resolve these problems and recover from their adverse consequences. This may be achieved with the use of sensors, signal processing and artificial intelligent (AI) techniques. This proposed research focuses on design, and fabrication of a hydraulic experimental set-up that allows fault emulation, and development of a model-based fault detection, diagnosis and real-time control scheme. Specifically, the objectives of the research are to:

- Analyze and select the best modeling approach, compromising between model accuracy, model complexity, and real-time detection and response effectiveness.
- Develop algorithms to characterize, isolate and correctly associate various faults to causes.
- Design an experimental set-up, which gives the flexibility to induce the proposed faults at any desired location in the system, and simultaneously does

not produce any superfluous affect due the arrangement, other than that induced by the simulator algorithm.

- Experimentally verify the theoretical propositions.
- Develop, verify and integrate fault detection and diagnosis module for hydraulic systems.
- Perform fine-tuning to obtain a trade-off between false alarms and detection rate.

In this thesis, Unscented Kalman Filter (UKF), a novel methodology inspired from Kalman filters, is utilized for health monitoring of the system. This methodology is a recursive estimator. This means that only the current measurement and the estimated state from the previous time step are required to compute the estimate for the current state. The significant characteristic of the UKF is that they are suitable for highly non-linear systems.

Faults affecting the reliability of hydraulic systems are the most critical in industrial applications. Four of the common faults in such systems will be studied. These are:

1) Dynamic friction due to the load. (Emulated by resistance from a pneumatic cylinder.)
2) Sudden loss of load.
3) Internal leakage of the actuator. (Emulated with a needle valve.)
4) External leakage of the actuator. (Emulated with two needle valves.)

Based on the model developed, the control command executed, and the measurements obtained on the response, Unscented Kalman filtering technique will be

used to determine the state errors or residuals. Devising practical and statistically viable thresholds, the residuals will be used to isolate a possible fault and to identify the probable cause. Once a degree of certainty is established, corrective actions can be taken. This may constitute a) modifying the control command, b) issuing a warning, or c) safely halting the operation if possible.

1.5 Organization of the Thesis

This thesis, which is conducted to meet the outlined scope, is organized in the following order. Chapter 1: The hydraulic systems along with their applications are introduced and also potential faults that may occur in the practical hydraulic systems are discussed. The objectives of the current research are also explained.

Chapter 2: The experimental hydraulic set-up is introduced and a state space model is developed and explained in detail. Simulations and tests are carried out in order to validate the developed state space model. Also, the frequency range of the system is discussed.

Chapter 3: fault diagnosis methods are surveyed and a basis for understanding the Kalman filter is provided in this chapter. Moreover, the Unscented Kalman filter, as the base of the fault diagnosis methodology in this research, is studied in detail. The fault monitoring scheme applied to the hydraulic test rig is developed and the simulation results are shown to confirm the satisfactory operation of the proposed algorithm.

Chapter 4: Condition monitoring of the hydraulic test rig is investigated. The results of the real-time state estimation are shown followed by the fault diagnosis discussions.

Chapter 5: The conclusions drawn from the investigation are presented, and the prospects for applications and further developments are discussed.

CHAPTER 2

System Modeling and Set-up Configuration

2.1 Introduction

This chapter describes the experimental set-up on which the condition monitoring is conducted. The investigated test rig is typical of the systems used in many industrial applications. It is composed of a group of essential hydraulic components including a pump, servo-valve, solenoid-valve, cylinder, needle-valve, relief-valve, and filter. Component specifications along with the non-linear dynamic equations are analyzed to develop a mathematical model of the system. A LabView™ interface is developed to issue control commands based on sensory data and perform real-time condition monitoring and fault diagnosis.

In Section 2.2 the test rig configuration is illustrated and its subsystems along with their operations are explained in detail. Then, all five potential faults that are emulated by the current scheme are discussed. Subsequently, the state space model

corresponding to the explained set-up is derived in Section 2.3. This mathematical model is further elaborated with the details of the various governing equations, function modeling, and all related parameters. In Section 2.4, the actual data acquired from the set-up is compared with the simulation results in order to validate the developed state space model.

2.2 Experimental Test Rig

The schematic diagram of the experimental set-up is shown in Figure 2.1. The entire system is divided into two subsystems: Pneumatic and Hydraulic subsystems. The hydraulic part is the main part of the system while the pneumatic subsystem is designed to emulate the dynamic friction load.

The pneumatic subsystem consists of an SMC five-way solenoid valve connected to an air pressure supply. This supply provides the constant pressure of 750 KPa. The solenoid valve receives the control signal from a PC equipped with a PCI-6024E data acquisition board. The asymmetric pneumatic cylinder controlled by this solenoid valve applies a force to the hydraulic actuator as an occurred fault for the hydraulic subsystem. The direction of this force is always opposite of the hydraulic actuator movement. To do so, as the hydraulic servo-valve pressurizes the retracting chamber (chamber 2 as illustrated in Figure 2.2), the pneumatic solenoid valve connects the supply line to retracting chamber of pneumatic cylinder and vice versa. This process emulates the dynamic friction load, which is common in practical servo-actuator systems. The magnitude of this force is 1162 N during the hydraulic actuator extraction period while it is 1042 N during the hydraulic actuator retraction period.

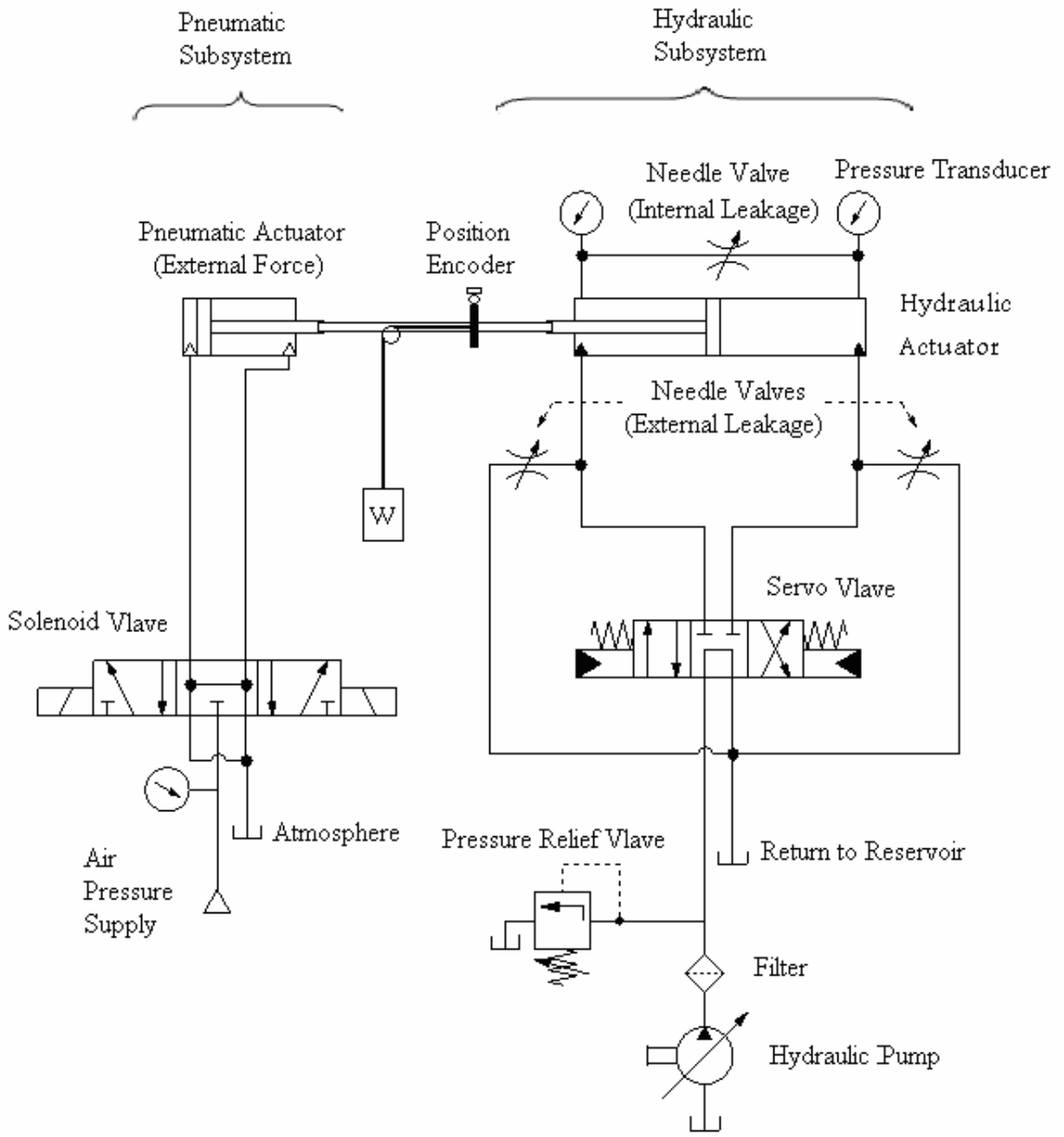

Figure 2.1: Schematic diagram of the experimental set-up

The hydraulic subsystem is powered by a pump supplying high-pressure hydraulic fluid to the actuator. In order to investigate a more general system modeling, an asymmetric cylinder rather than a symmetric one is employed as the actuator. As shown in Figure 2.2, chambers are referred to as chamber 1 and chamber 2, and are connected to an Atchley Controls® servo-valve. Its control signal range is from -100 mA to 100 mA,

which is received from a computer equipped with the LabView™ software. Analog and digital electronic units are shown schematically in Figure 2.3. Three sensors are installed in the set-up to measure the required states. Two pressure transducers are mounted to measure the pressure in both chambers. A position encoder measures the displacement of the actuator. All these signals are transmitted to the PC via the PCI-6024E data acquisition board, and subsequently the command signals are sent to servo-valve from the PC.

Points of leakages and external forces as potential faults are illustrated in Figure 2.2. Flows of q_1 and q_2 to chambers 1 and 2 respectively are controlled by the input current I_a of the servo-valve. Since the servo-valve has a symmetric spool, the positive direction for the spool movement is arbitrarily defined. As for the asymmetric cylinder, the positive direction for the actuator movement is outward to the left.

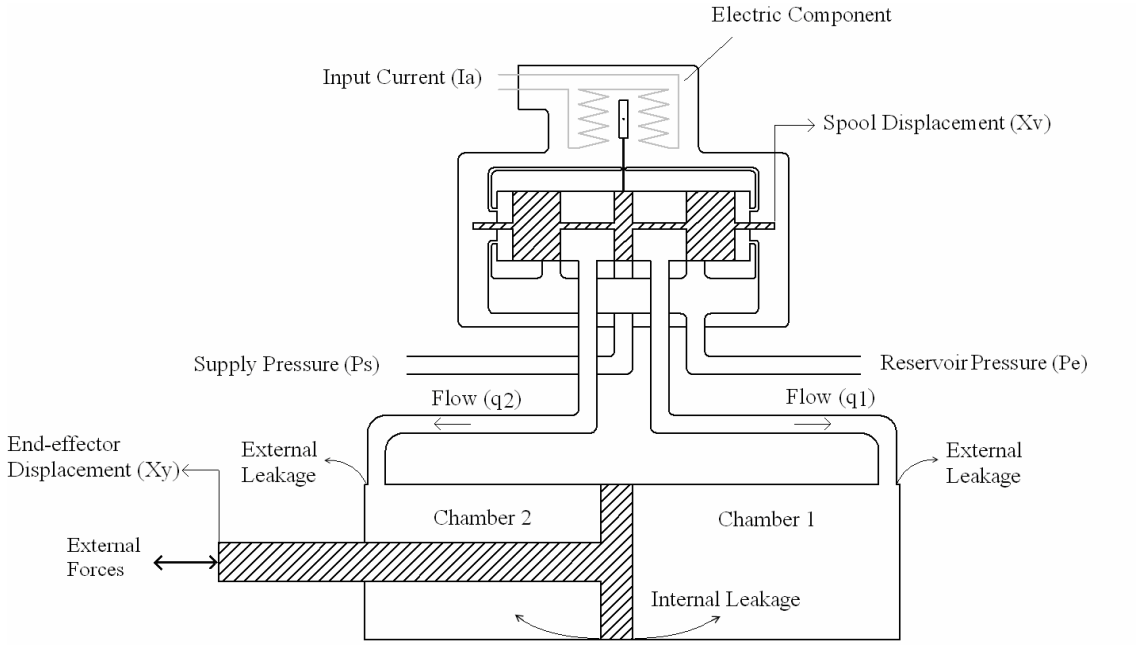

Figure 2.2: Servo-actuator functional diagram

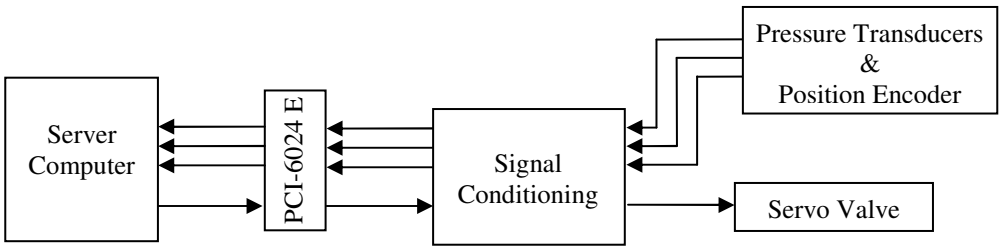

Figure 2.3: Schematic diagram of the control units

The set-up is designed to produce common faults in the hydraulic systems. Figure 2.4 shows a photograph of the experimental test rig. All three leakages are emulated by means of three needle valves with the same characteristics. These needle valves are shown in Figure 2.5a. On each chamber, there is a pressure transducer along with a visual gage for safety purposes. One needle valve is mounted as the bypass for the cross-port leakage emulation. As shown in Figure 2.5b, a pneumatic cylinder, a position encoder, an LVDT, and an external load are connected to the hydraulic end-effector. The LVDT is used to mark the origin of the actuator, while the position encoder is employed to measure the displacement from this origin. The actuator stroke is 10 cm and the origin of x_y is located at the point where the ram is fully retracted. Since the external load is emulated by means of two suspended weights, due to the gravity, its effect is a force applied on the actuator asymmetrically. This force resists the piston displacement during the retracting period while it accords with the movement during the extracting period. Sudden loss of these weights is a scenario that will be discussed as another occurred fault in the system in section 4.2.2.2.

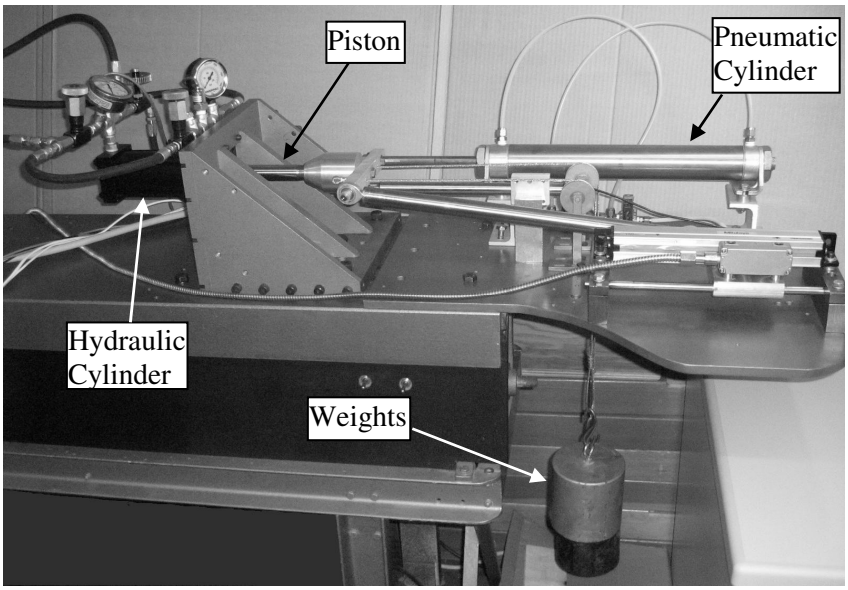

Figure 2.4: Hydraulic test rig

The closed-loop controller regulates the characteristics of the hydraulic test rig. To validate the performance of the proposed closed-loop system, the set-up is excited with a sinusoidal reference signal that the end-effector position should follow. A low frequency sinusoidal signal, $r = 0.05 + 0.02\sin(0.4\pi t)$ meter, is considered as the reference signal for a period of 50 seconds. Due to the digital computing pace limits, the sampling time is chosen as 20 ms in this research. Figure 2.6 shows the reference signal along with the measurement signals. With a comparison between Figures 2.6a and 2.6b, it can be observed that the end-effector tracks the reference signal satisfactorily; however, there is a phase difference of around $\pi/4$, as well as a 4% amplitude offset. Additionally, Figures 2.6c and 2.6d show that the pressure in chamber 2 is much higher than that at chamber 1. The reference signal is symmetrical around the origin therefore the servo-valve transmits higher pressure to chamber 2 because this chamber has less effective area than that of chamber 1. Moreover, with reference to the hydraulic system schematic

diagram shown in the Figure 2.1 the asymmetric external load intensifies the pressure in chamber 2.

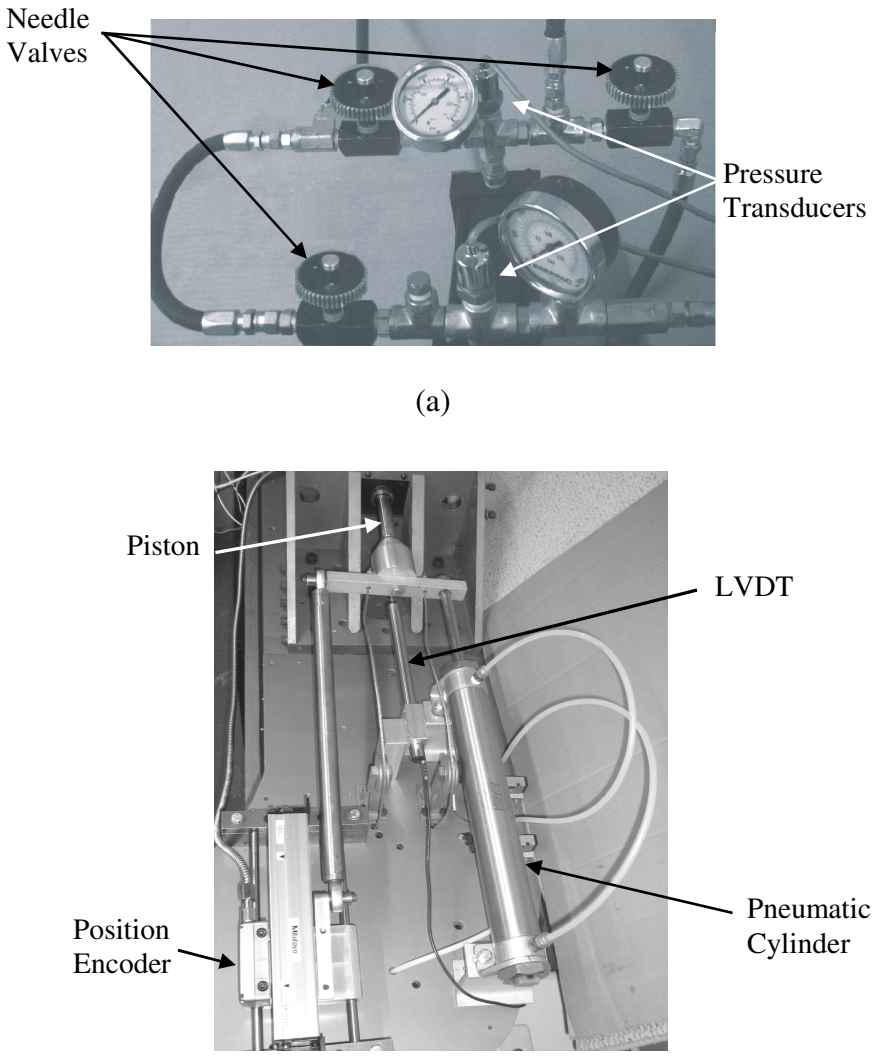

Figure 2.5: Hydraulic test rig in more detail, (a) Hydraulic circuit, and (b) Pneumatic circuit and end-effector attachments

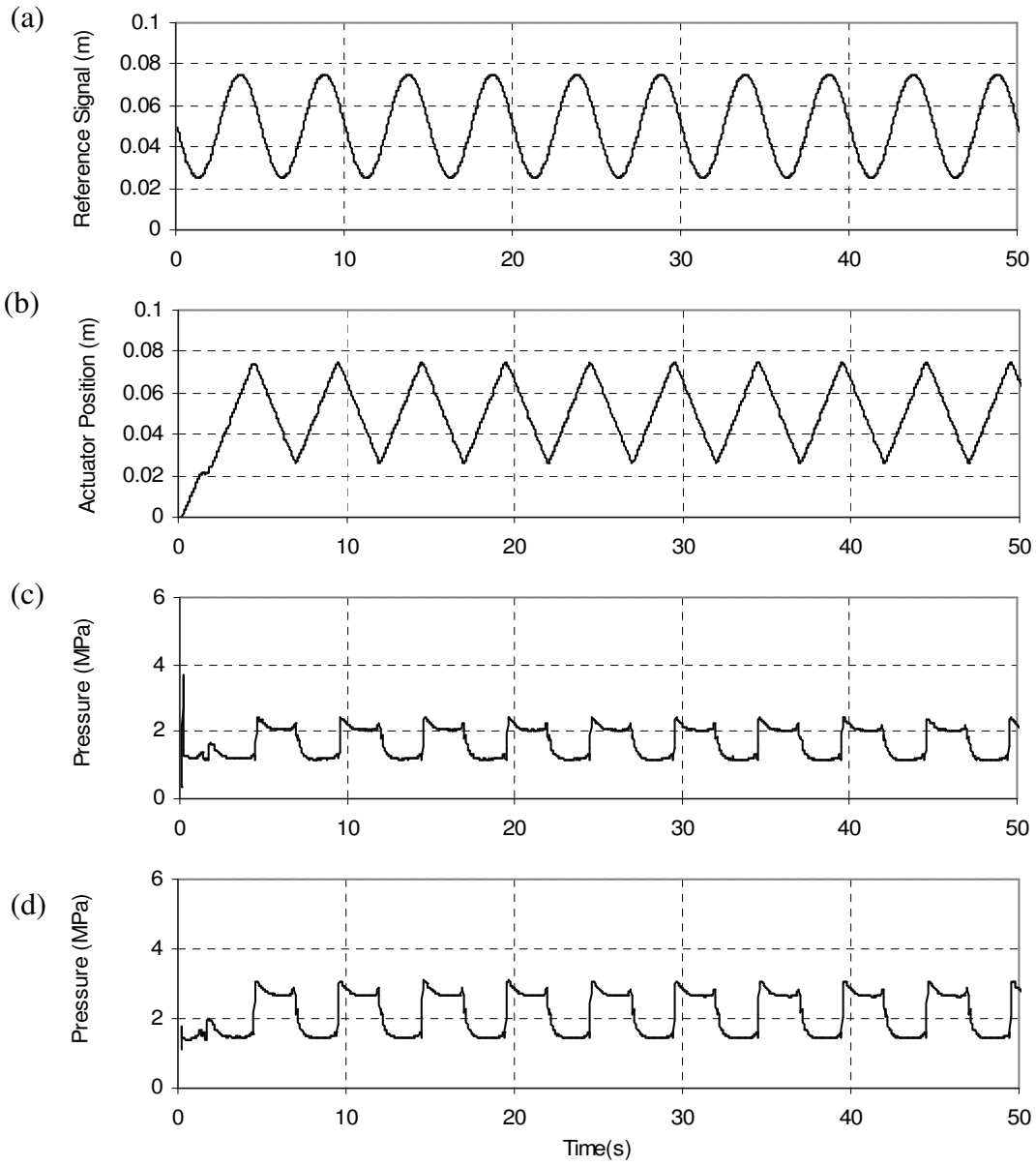

Figure 2.6: The test rig characteristics, (a) actuator position reference signal and resulting (b) end-effector displacement, (c) Pressure in chamber 1, and (d) Pressure in chamber 2

2.3 System Modeling

2.3.1 Governing Equations

The dynamics of almost all practical hydraulic components can be appropriately described by the equations presented by Merritt [2]. In this research, understanding the dynamic features of the actuator and the servo-valve are imperative. The flow through the servo-valve is proportional to the square root of the pressure drop across the port and the area of the valve opening. The valve opening area is proportional to the spool displacement and therefore by applying a linear orifice area gradient related to the spool displacement, the following expression can be used to represent the flow equations of the servo-valve:

$$\begin{cases} q_1 = -C_d \omega x_v \left(\sqrt{\left| \frac{2}{\rho}(p_1 - P_e) \right|} \right) sign(p_1 - P_e) \\ q_2 = C_d \omega x_v \left(\sqrt{\left| \frac{2}{\rho}(P_s - p_2) \right|} \right) sign(P_s - p_2) \end{cases} \quad x_v \geq 0$$

$$\begin{cases} q_1 = -C_d \omega x_v \left(\sqrt{\left| \frac{2}{\rho}(P_s - p_1) \right|} \right) sign(P_s - p_1) \\ q_2 = C_d \omega x_v \left(\sqrt{\left| \frac{2}{\rho}(p_2 - P_e) \right|} \right) sign(p_2 - P_e) \end{cases} \quad x_v < 0 \qquad (2.1)$$

where:

q_1, q_2: flow from the servo-valve to chamber 1 and chamber 2

P_s, P_e: supply and return line pressures

p_1, p_2: pressures in chamber 1 and chamber 2

x_v: the servo-valve spool displacement

C_d, ω: orifice coefficient of discharge and orifice area gradient

ρ: density of the hydraulic oil

It is assumed that the rod and the piston of the hydraulic cylinder are rigid, and the oil on either side of the piston is compressible. As this compressibility is proportional to the volume in which pressure acts, the rate of the change of volumes within the actuator may be expressed as:

$$\begin{cases} q_{c1} = \dfrac{1}{\beta}\left(V_0 + A_1\left(x_y - X_{\min}\right)\right)\dot{p}_1 \\ q_{c2} = \dfrac{1}{\beta}\left(V_0 + A_2\left(X_{\max} - x_y\right)\right)\dot{p}_2 \end{cases} \tag{2.2}$$

where:

β: effective bulk modulus of the hydraulic fluid

A_1, A_2: effective piston areas of chamber 1 and chamber 2

x_y: actuator position

X_{max}, X_{min}: positions when the piston is fully extended and fully retracted

V_0: volume of the fluid trapped in the supply pipes connected to each chamber (it is assumed that this volume is identical for both chambers)

The continuity equations for hydraulic flows of the actuator are applied to determine a relationship between chamber flows, chamber pressures, and the piston velocity. By considering the compressibility issue from the preceding equation, the following descriptions are held for the flows of the chambers.

$$\begin{cases} q_1 = A_1\dot{x}_y + \dfrac{1}{\beta}\left(V_0 + A_1\left(x_y - X_{\min}\right)\right)\dot{p}_1 \\ q_2 = -A_2\dot{x}_y + \dfrac{1}{\beta}\left(V_0 + A_2\left(X_{\max} - x_y\right)\right)\dot{p}_2 \end{cases} \tag{2.3}$$

Equations 2.1 and 2.3 are combined to eliminate the flow parameters from the equations. By solving the obtained relationship for $\dot{p}_1$ and $\dot{p}_2$, we achieve:

$$\begin{aligned} \dot{p}_1 &= \begin{cases} \dfrac{\beta}{V_0 + A_1(x_y - X_{\min})}\left[C_d\omega x_v\sqrt{\dfrac{2}{\rho}(p_1 - P_e)} - A_1\dot{x}_y\right] & x_v \geq 0 \\ \dfrac{\beta}{V_0 + A_1(x_y - X_{\min})}\left[C_d\omega x_v\sqrt{\dfrac{2}{\rho}(P_s - p_1)} - A_1\dot{x}_y\right] & x_v < 0 \end{cases} \\ \dot{p}_2 &= \begin{cases} \dfrac{\beta}{V_0 + A_2(X_{\max} - x_y)}\left[C_d\omega x_v\sqrt{\dfrac{2}{\rho}(P_s - p_2)} - A_2\dot{x}_y\right] & x_v \geq 0 \\ \dfrac{\beta}{V_0 + A_2(X_{\max} - x_y)}\left[C_d\omega x_v\sqrt{\dfrac{2}{\rho}(p_2 - P_e)} - A_2\dot{x}_y\right] & x_v < 0 \end{cases} \end{aligned} \tag{2.4}$$

The position of the flow controlling spool valve as a function of the drawn current can be characterized by a quadratic system:

$$K_{sp}u = \ddot{x}_v + \omega_n d_m \dot{x}_v + \omega_n^2 x_v \tag{2.5}$$

where:

K_{sp}: spool valve positioning gain

ω_n: natural frequency of the spool dynamics

u: valve input current

d_m: damping ratio

The dynamics of the actuator is modeled based on the summation of the forces acting on the piston of the cylinder. The following equation can be expressed:

$$\sum f = M_e \ddot{x}_y = A_1 p_1 - A_2 p_2 - f_f + F_{ext} \tag{2.6}$$

where:

M_e: combined effective mass of the objects moving with the ram

f_f, F_{ext}: actuator friction and external forces

As illustrated in Figure 2.1, the ram pulls up a mass, M_a = 25 kg, during its retraction. For the hydraulic system this weight acts as an external force (F_{ext} = 245 N). Moreover, it is assumed that this weight moves along with the ram and therefore its mass should be added to the effective mass of the moving objects. Also, the pneumatic cylinder ram and the position encoder are attached to the end-effector. Then as a result M_e = 33 kg.

Friction is an unavoidable factor in moving machinery and thus it has to be studied as a part of dynamics. Friction is a non-stationary and non-linear force that depends on many physical parameters and even environmental situations. As an instance when two sliding materials are lubricated, different sliding speed causes different film thickness of the lubricant and therefore friction characteristics may change. Not only because of the challenges of the friction modeling but also due to its significant impact on the dynamic of the system, there has been considerable interest in this field. Karnopp [17] proposed a typical stick-slip friction model in mechanical dynamic systems. Laval [18] improved the Karnopp model and his proposition is adopted in this study to model the friction inside of the hydraulic cylinder. His model is expressed as:

$$f_f = \begin{cases} [f_{st} - (f_{st} - f_{sl})(1 - e^{-C|\dot{x}_y|})]sign(\dot{x}_y) + d\dot{x}_y & \dot{x}_y \neq 0 \\ f_{st} & \dot{x}_y = 0 \end{cases} \tag{2.7}$$

where:

f_{st}, f_{sl}: static and kinetic friction forces

C: lubrication coefficient

d: effective damping ratio

In order to produce reliable numerical results, all above parameters and physical quantities should be known initially. The parameters of the current system are classified into two sets. Parameters of the first set such as effective bulk modulus of the fluid are those that are either specified by the manufacturer or measurable directly. On the other hand, some parameters, which are categorized as the second group, are neither measurable directly nor specified by the manufacturer, such as the static friction, and hence must be determined by a set of experiments and measurements through the system states.

To accurately estimate the friction of the actuator, unloaded set-up is run in different scenarios to evaluate both static and kinetic frictions. To determine the kinetic friction parameter, f_{sl}, the ram is run in several certain velocities. With reasonably good precision, it is assumed that these movements have no acceleration (except at start and stop) and hence the calculated actuation forces during the ram motions give an indication of the kinetic friction. The results of these experiments are shown in Figure 2.7, where actuator friction forces are seen to stay reasonably constant for speeds over 0.015 m/s in either direction. As an instant of experimental result, Figure 2.6 shows the actuator movement from which it can be derived that the average velocity of the actuator is around 0.02 m/s. Because this is more than 0.015 m/s, the steady friction force can be

chosen as the kinetic friction value. From the Force-Velocity curve (Figure 2.7) the actual magnitude of the kinetic friction can be appraised as 0.140 kN, which is the average of the actuation force values at the velocity of 0.015 m/s in either direction.

To recognize the static friction, $f_{st,}$ the input current is regulated to make the ram start moving. To do so, the current is increased slowly until the ram starts to move. For the sake of simplicity, since the ram starts moving slowly, the acceleration is ignored. This experiment is carried out in three different locations along the cylinder for both retracting and extracting directions and the applied actuation force is calculated in each trial run. Subsequently, the average of these six force values is taken to represent the approximate static friction, which is obtained as 0.295 kN.

There are two other parameters in the friction formulation that should be dealt with: the effective damping ratio (d) and the lubrication coefficient (C). The mathematical friction model (equation 2.7) is plotted for different values of d and C (not all calculations are reproduced here). Both values are positive and also in all surveyed literature in which this model of the friction is investigated, the inverse of the lubrication coefficient is a positive value less than one tenth. We hereby try to fit the mathematical model to the experimental data (Figure 2.7) in a trial and error approach. The values of d and C from the best fitted curve are chosen for the state space model parameters. The damping ratio, d, is 250 N.s/m, while the lubrication coefficient, C, is 28 s/m.

The following table shows all actual parameters employed in the state space model.

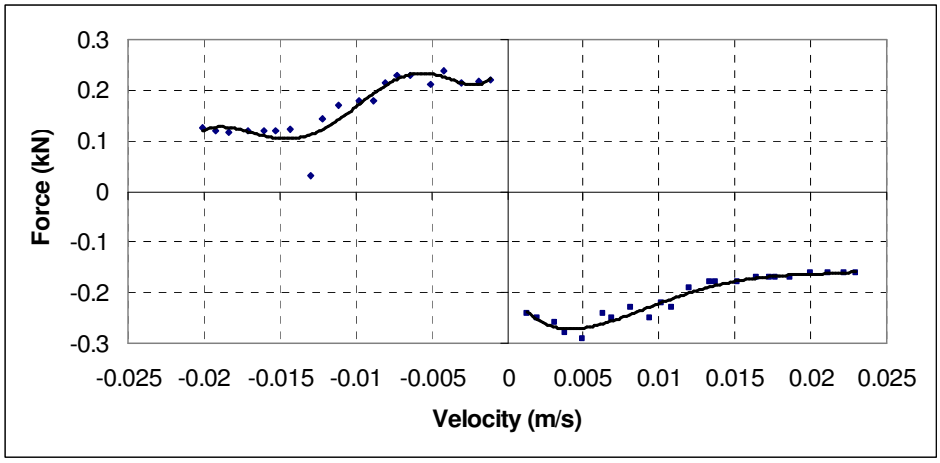

Figure 2.7: Experimental results in actuator friction investigation

Table 2.1: The numeric values of the hydraulic set-up parameters

$A_1 = 31.7 \times 10^{-4}\ m^2$	$f_{st} = 295\ N$	$v_0 = 0.001\ m/s$
$A_2 = 26.6 \times 10^{-4}\ m^2$	$f_{sl} = 140\ N$	$\omega = 0.02\ m^2/m$
$M_e = 33\ kg$	$C = 28\ s/m$	$\beta = 6.89 \times 10^8\ Pa$
$X_{min} = 0\ m$	$k_{sp} = 3.003 \times 10^{-5}\ V/m$	$\rho = 857\ kg/m^3$
$X_{max} = 0.1\ m$	$\omega_n = 600\ rad/s$	$P_s = 6.5\ MPa$
$d = 250\ N.s/m$	$d_m = 0.7$	$P_e = 0\ MPa$
$C_d = 2.605 \times 10^{-2}$	$V_0 = 18.09 \times 10^{-6}\ m^3$	$F_{ext} = 245\ N$

2.3.2 State Space Model

The state vector of the state space model consists of six variables, which are defined as the following:

$$\dot{x} = \begin{bmatrix} x_1 & x_2 & x_3 & x_4 & x_5 & x_6 \end{bmatrix}^T = \begin{bmatrix} x_v & p_1 & p_2 & x_y & \dot{x}_y & \dot{x}_v \end{bmatrix}^T \qquad (2.9)$$

In order to acquire the state space model, $\dot{x}$ should be derived. Having noted the definition of x_1 and x_6, the following expression can be written:

$$\dot{x}_1 = x_6 \tag{2.9}$$

In order to determine functions for $\dot{x}_2$ and $\dot{x}_3$, equation 2.4 can be recast as the following:

$$\begin{aligned}
\dot{x}_2 &= \begin{cases} \dfrac{\beta}{V_0 + A_1(x_4 - X_{\min})}\left[C_d \omega x_1 \sqrt{\dfrac{2}{\rho}(x_2 - P_e)} - A_1 x_5\right] & x_1 \geq 0 \\ \dfrac{\beta}{V_0 + A_1(x_4 - X_{\min})}\left[C_d \omega x_1 \sqrt{\dfrac{2}{\rho}(P_s - x_2)} - A_1 x_5\right] & x_1 < 0 \end{cases} \\
\dot{x}_3 &= \begin{cases} \dfrac{\beta}{V_0 + A_2(X_{\max} - x_4)}\left[C_d \omega x_1 \sqrt{\dfrac{2}{\rho}(P_s - x_3)} - A_2 x_5\right] & x_1 \geq 0 \\ \dfrac{\beta}{V_0 + A_2(X_{\max} - x_4)}\left[C_d \omega x_1 \sqrt{\dfrac{2}{\rho}(x_3 - P_e)} - A_2 x_5\right] & x_1 < 0 \end{cases}
\end{aligned} \tag{2.10}$$

and $\dot{x}_4$ can be easily expressed as:

$$\dot{x}_4 = x_5 \tag{2.11}$$

To derive an expression for $\dot{x}_5$, f_f from equation 2.7 can be substituted in the dynamic model of the actuator (equation 2.6) and then solved to obtain an equation for $\ddot{x}_y$. Generally, a threshold is considered for zero in numerical computations, therefore a threshold as v_0 is designated in the expression for f_f. The following shows the $\dot{x}_5$ formulation in the state space model:

$$\dot{x}_5 = \frac{1}{M_a}(A_1 x_2 - A_2 x_3 - f_f + F_{ext}) \tag{2.12}$$

in which:

$$f_f = \begin{cases} [f_{st} - (f_{st} - f_{sl})(1 - e^{-C|x_5|})]sign(x_5) + dx_5 & |x_5| > v_0 \\ f_{st} & |x_5| \le v_0 \end{cases} \quad (2.13)$$

By solving the equation 2.5 for $\ddot{x}_v$, the following expression holds for $\dot{x}_6$:

$$\dot{x}_6 = -d_m \omega_n x_6 - \omega_n^2 x_1 + k_{sp} u \quad (2.14)$$

2.4 Model Validation

Any mathematical model should be validated in order to ascertain that the differences between the measured states from the practical system and the simulated states from the state space modal do not exceed a certain threshold for a similar input signal. For hydraulic systems, these thresholds are approximately 10% of the actual measurements according to most literature such as [19-21]. These errors are considered as model uncertainties presented by the process noise in the proposed fault diagnosis algorithm that will be explained in Chapter 3.

In the current research the moving average method is used to study the error signals. In this method, the average of a number of data is taken at each discrete time increment. By applying this algorithm to error data, the effects of extra noises and transient errors on the error signal diminish. The moving average of the errors (MAEs) at k^{th} time step is calculated by the following expression:

$$e_k = \frac{\sum_{i=k-m}^{k} |e_i|}{m} \quad (2.15)$$

in which m is the number of previous error data from which the average is calculated at each time step. e_i is the error data at the i^{th} time step. In the current study, m is chosen as

250 considering the sampling time and the reference signal frequency. As explained in section 2.2, the sampling time is 20 ms and the frequency of the reference signal is 0.4π rad/sec. Thus by choosing *m* as 250, the MAE is calculated for a complete motion period, a full retraction and extraction, at each time step.

2.4.1 Experimental Results

In order to validate the state space model, a low frequency sinusoidal signal, $r = 0.05 + 0.02\sin(0.4\pi t)$ meter, is applied to both mathematical model and the experimental test rig as the position reference signal for a period of 60 seconds. Figures 2.8 and 2.9 illustrate the characteristics of the pressures in chamber 1 and chamber 2, respectively. Both measured and simulated pressures are shown and also the error between the model and the system for the corresponding state is represented. It can be observed visually that the simulated and the measured pressures are so close to each other and the errors converge to satisfactory values. The MAE is 0.12 MPa for chamber 1 and 0.14 MPa for chamber 2, which are within 10% of the actual measurements. Figure 2.10 depicts both actuator displacement trajectories from sensor signal and state space model computation as well as the corresponding error signals. This figure shows that the simulated trajectory adequately matches the measured one. The MAE signal, which has a steady value around 2 mm, stays within 10% of the actual measurements of the actuator movement.

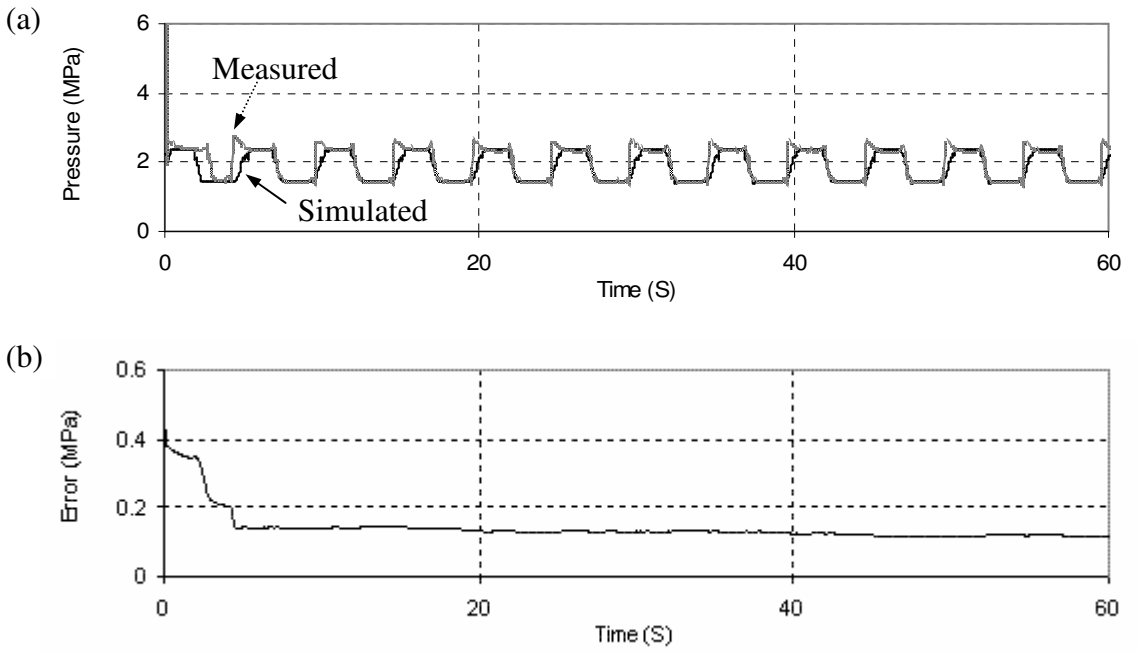

Figure 2.8: (a) Simulated and measured values of the pressure in chamber 1, (b) MAE between simulated and measured values

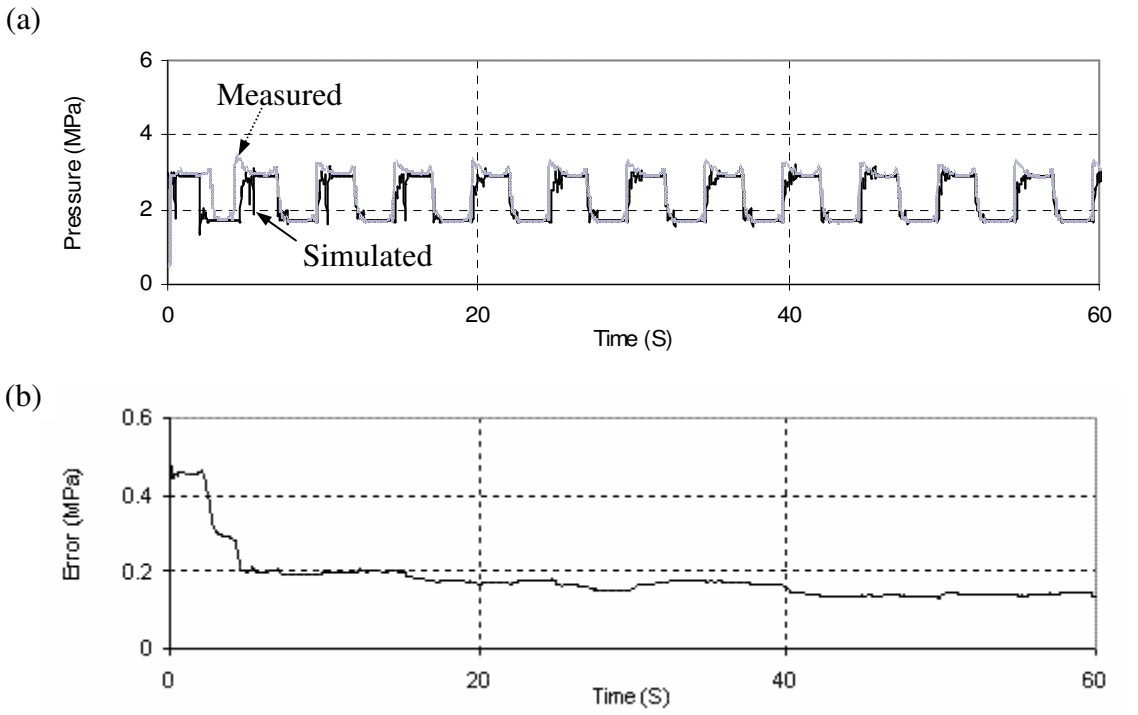

Figure 2.9: (a) Simulated and measured values of the pressure in chamber 2, (b) MAE between simulated and measured values

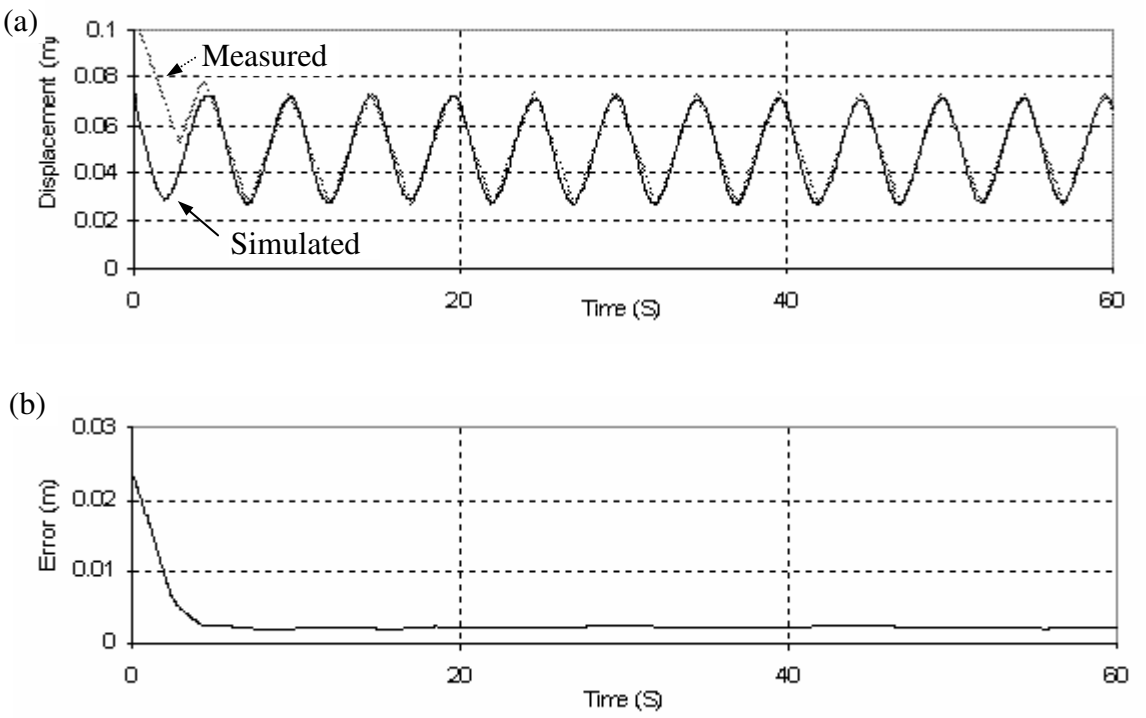

Figure 2.10: (a) Simulated and measured values of the actuator displacement, (b) MAE between simulated and measured values

2.4.2 Frequency Range

To compare the frequency responses of the practical system and the state space model, a sinusoidal position reference signal with a time varying frequency and constant amplitude is applied to the servo-valve and the state space model. The reference signal is $r = 0.05 + 0.02\sin(0.3(1 + \frac{t}{4})t)$ meter. The error signals between measured and simulated results are shown in Figures 2.11 to 2.13. All three measurands are studied in the frequency range between 0.05 to 0.8 Hz, which is a typical range of practical operating frequencies for hydraulic systems. The simulation errors of the state space model increase by increasing the input frequency as it can be observed from the figures.

Nevertheless, the error signals still stay within the satisfactory boundary. In this study, all experiments are carried out at the frequency of 0.2 Hz.

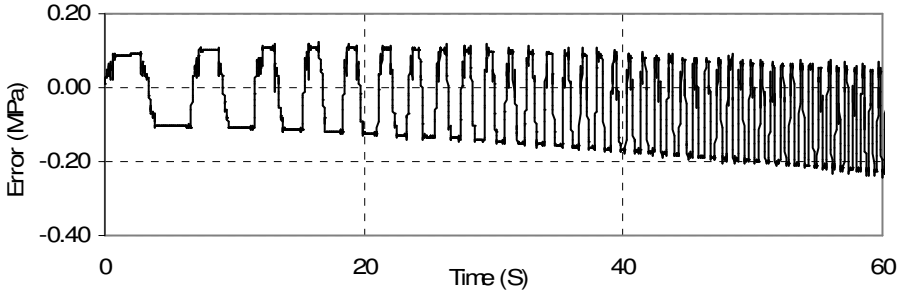

Figure 2.11: Error signal between measured and simulated pressure of chamber 1

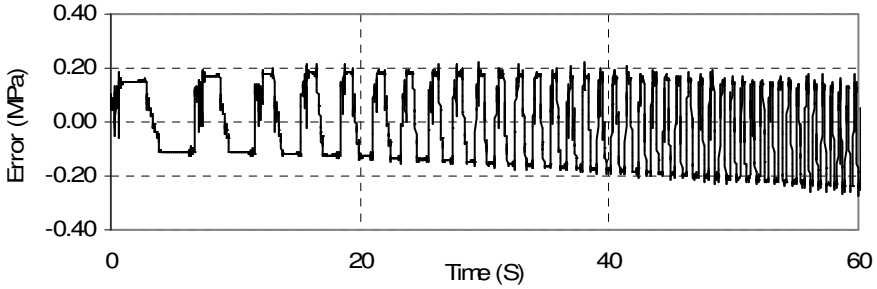

Figure 2.12: Error signal between measured and simulated pressure of chamber 2

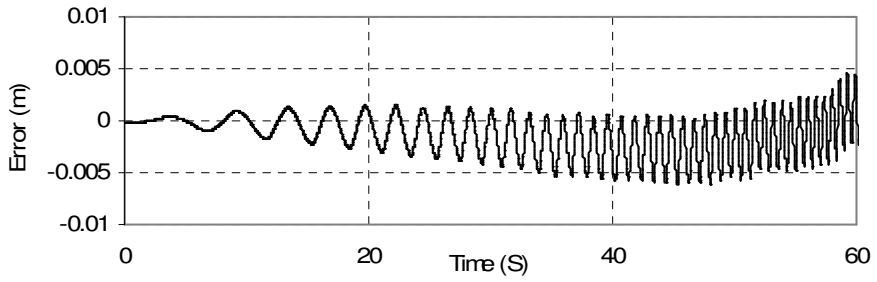

Figure 2.13 Error signal between measured and simulated displacement

2.4.3 Repeatability of the Experiments

It is essential that the system measurements are repeatable within an acceptable margin in any experimental study. This is necessary in interpreting the results and

drawing conclusions. In all the tests, the operating conditions such as fluid temperature, supply pressure, operating scheme, etc remain almost constant. The operating supply pressure was approximately 6.50 MPa and the laboratory temperature was set to be around 20˚C.

Repeatability of the pressure in chamber 1 is illustrated in Figure 2.14 as an example. The test rig was run at different times and three sets of measurements were collected for the same operating conditions. It can be verified visually that the data of this particular state are very similar from test to test. All four data sets show similar trends, time periods and magnitudes. Variation between the traces is very small. It is perceived that the values of five performance indicators, minimum, maximum, mean, standard deviation, and range, for these three data sets are very close, all varying within 0.8%. These indicators suggest that the data repeatability is acceptable.

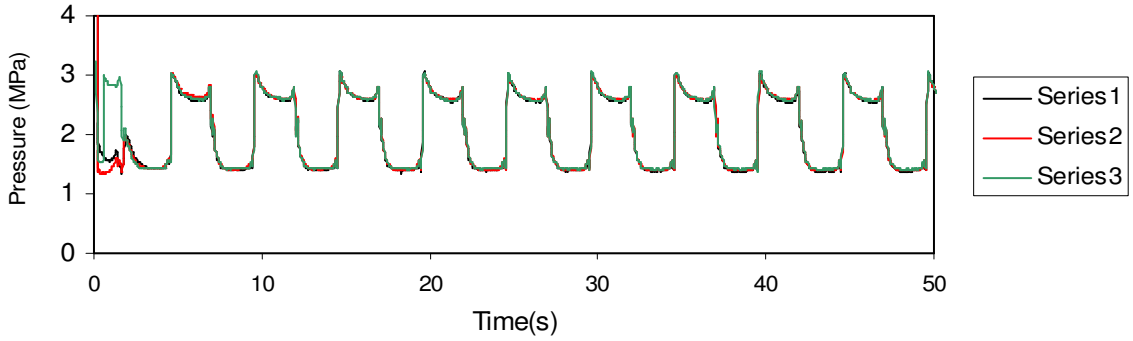

Figure 2.14: Pressure repeatability

CHAPTER 3

Implementation of a Fault Monitoring Technique

3.1 Introduction

A fault is a deviation of a desirable characteristic property leading to the inability to fulfill an intended purpose. Practically, it is assumed that the system is healthy and no fault is present at the beginning but takes place some time, with magnitude, type and time of occurrence being unknown [22]. Generally, faults occur in two different manners: a) step functions such as when the end-effector is obstructed by an object or b) ramp functions such as leakage or deterioration of a device. It is essential to distinguish the difference between noise and fault. Customarily, any noise is considered as a random zero-mean signal, which could originate from any element of the plant especially from sensors; meanwhile, any non-zero-mean disturbance is treated as a fault.

In this chapter the development and implementation of the condition monitoring technique for the current study are investigated. The material in this chapter is organized

as follows; initially, in Section 3.2, an overview of fault categories in dynamic systems is given. Afterwards, fault diagnosis approaches are classified and explained in Section 3.3. A general Kalman filter algorithm is explained in Section 3.4. Sections 3.5 and 3.6 outline the Unscented Kalman filter and its application in the present system.

3.2 Classification of Faults

Faults may be classified into the following groups [23]:

1. Additive faults: they are unknown inputs, which vary the plant outputs independently of the known inputs. The existence of an external force or friction load as a fault is a certain instance of this class of faults. Additive faults, known as Error-In-Variable (EIV), [24] do not depend on whether other faults have occurred or not therefore they can easily be detected.

Sensor output signals are generally affected by non-zero-mean signals and hence they differ from the actual values of measurands. These faults are usually considered as additive faults (even though some sensor faults such as complete failure may be better designated as another class, which is "multiplicative faults"). The following model describes the general sensor signals from the healthy system:

$$\begin{cases} u(t) = \bar{u}(t) + \tilde{u}(t) \\ y(t) = \bar{y}(t) + \tilde{y}(t) \end{cases} \tag{3.1}$$

where $u(t)$ is the system input signal and *y(t)* is the actual system output, $\bar{u}(t)$ and $\bar{y}(t)$ are fault-free sensor signals, $\tilde{y}(t)$ and $\tilde{u}(t)$ are corresponding noises. Moreover, sensor signals from faulty systems can be modeled as the following:

$$\begin{cases} u(t) = \bar{u}(t) + \tilde{u}(t) + f_u(t) \\ y(t) = \bar{y}(t) + \tilde{y}(t) + f_y(t) \end{cases} \tag{3.2}$$

in which $f_u(t)$ and $f_y(t)$ are the models of the fault situations.

2. Multiplicative faults: they may turn up as parameter deviations within the systems, which lead to the system output changes [25, Chapter 1]. These deviations depend on the magnitudes of the plant control inputs. Deteriorations of the system elements such as loss of power are categorized as multiplicative faults. This type of faults can be modeled as the following [26]:

$$\begin{cases} \dot{x}(t) = (A + \Delta A)x(t) + (B + \Delta B)u(t) \\ y(t) = (C + \Delta C)x(t) + (D + \Delta D)u(t) \end{cases} \tag{3.3}$$

in which A, B, C, and D are the state space model matrices and Δs show the deviations from the healthy system matrices resulting from the parameter changes.

3.3 Overview of Fault Diagnosis Approaches

There is an abundance of literature on process fault diagnosis ranging from artificial intelligence to analytical methods and statistical approaches. Fault diagnosis methods are usually classified due to the type of the usage of *a priori* process knowledge. The *a priori* knowledge is the relationship between the failures and the observations, which may be obtained either explicitly or from any source of domain knowledge. Based on the knowledge that requires *a priori,* fault diagnosis techniques surveyed in [27-29] can be categorized into two general classes; model-based and model-free (data driven) methods.

From a modeling perspective, there are methodologies that require accurate process models called quantitative models. At the other end of the spectrum, there are methodologies that do not require any form of model information and rely only on previous process data [30].

Given the process knowledge, there are various methods that can be employed to perform diagnosis. A taxonomy of major fault diagnosis techniques is shown in Fig. 3.1.

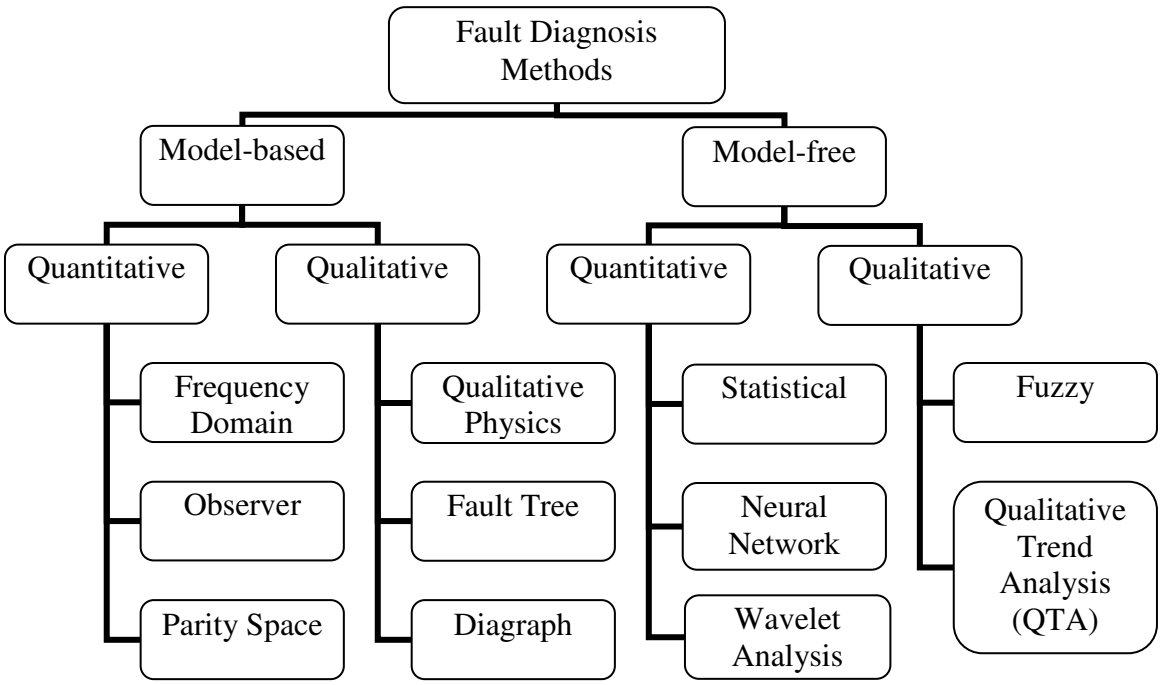

Figure 3.1: Classification of fault diagnosis methods

3.3.1 Model-based Fault Diagnosis Approaches

All model-based methodologies can be categorized into two major groups: qualitative and quantitative. The models of the systems are usually developed based on the fundamental understanding of the physics of the processes. In a quantitative approach

the fundamentals of the dynamic systems are demonstrated in a mathematical model in which some functions show the relationship between the system inputs and outputs. On the other hand, in a qualitative model the fundamental system relationships are expressed by qualitative functions.

3.3.1.1 Quantitative Model-based Methods

Most studied reported in literature working on quantitative model-based approaches develop a state space model of the system where residual errors can be generated. These techniques can be broadly classified into frequency domain, observer, and parity space classes.

Frequency Domain Approach

The basic idea behind the frequency domain approaches is to generate residuals via factorization of the transfer functions of the dynamic systems. Frank and Ding [31] studied a methodology in frequency domain for robust residual generation.

Observer Approach

Residuals can also be generated by estimation of the system outputs from the sensor data by using appropriate observers. Observer-based residual generators for linear systems were developed by Chen and Patton in [32], they also studied the correlation between factorization-based and observation-based residual generators. Regarding the observer criteria, these approaches may be classified as a) fixed (Chapter 13 of [33]) or adaptive [34], b) reduced [35] or full-order [36], and c) linear [37] or non-linear [38].

Parity Space Approach

Parity space methods rearrange the model of the system and examine the consistency of the model with sensor data and known system inputs. Willsky [39] introduced dynamic parity relations for failure detection.

3.3.1.2 Qualitative Model-based Methods

Based on various forms of qualitative knowledge used in fault diagnosis, qualitative model-based approaches can be classified into fault trees, digraphs and qualitative physics classes.

Qualitative Physics Approach

Qualitative physics is an area of artificial intelligence, which is concerned with reasoning about the behavior of physical systems. In fault diagnosis applications, qualitative physics knowledge is represented in two main groups. In the first group, qualitative equations (behavior) are derived from the differential equations. Umeda et al. [45] developed a fault detection methodology whose knowledge for diagnosis is based on qualitative physics. In the second group, the qualitative equations (behavior) are derived from ordinary differential equations (ODEs). Sacks [46] was the first who examined piece-wise linear approximations of non-linear differential equations by means of a qualitative mathematical regulator to infer the qualitative properties of a dynamic system.

Fault Tree Approach

Fault trees are commonly formed of layers of nodes and usually applied in analyzing of the system reliability. These logic trees propagate faults to the next level of layers. Different logic operations such as “AND” and “OR” are performed at each node

for propagation. He et al. [40] developed a methodology to accurately assess the system reliability with limited statistical data. They used fault tree analysis based on the fuzzy logic. Fault trees have been used in a variety of risk assessment and reliability analysis. Tartakovsky [41] estimated the probabilities of the system failures by means of uncertainty quantification techniques. Then, applied fault tree analyses to combine these probabilities in order to estimate the risk of the system failures.

Digraph Approach

Generally, a digraph is a graph, which includes directed arcs between nodes. And a signed diagraph (SDG) is a digraph in which these directed arcs are designated with either a positive or a negative sign. SDGs have been widely used to represent qualitative models or cause-effect relationships and also in the form of causal knowledge, they are employed to diagnose the process faults. The first development of the SDG for fault diagnosis was reported by Iri et al. [42]. They derive a cause-effect graph (CE graph) from SDG. Vedam and Venkatasubramanian [43] developed an SDG approach for multiple fault detection. Han et al. [44] incorporated the fuzzy set theory into SDGs to provide an accurate resolution of fault origin.

3.3.2 Model-free Fault Diagnosis Approaches

Model-free Fault diagnosis approaches are based on the historical process data rather than the models of the systems. From another point of view, these methodologies extract the feature characteristics from the previous data. Based on whether the knowledge about process characteristics is required or not, one can perform either qualitative or quantitative feature extraction.

3.3.2.1 Quantitative Model-free Methods

There are a notable number of methods, which are employed in decision making by the use of quantitative information without any necessity for system modeling. These can be categorized into two main classes: non-statistical methods such as neural network, and statistical methods such as Partial Least Squares (PLS).

Statistical Approach

Essentially, faults can be diagnosed by considering the combination of the instantaneous estimates of the pattern recognition over time. Historical information about the properties of the system failure mode is used and hence fault diagnosis can be treated in a statistical pattern recognition framework.

The extensive improvement in computing power of softwares has had an increasing impact on the practical applications of statistical science. The applications of statistical development in fault diagnosis area have been comprehensively studied in the literature. Kresta et al. [47] gave an overall overview of statistical monitoring in process analysis. They introduced a basic technique of using the PLS and PCA (Principal Component Analysis) to efficiently monitor the fulfillment of large processes and to quickly detect process changes. Qin and Li [48] studied a methodology based on the PCA for sensor fault detection. A non-linear PCA method for batch processes has been developed by Dong and McAvoy [49].

Neural Network Approach

A neural network consists of several processing modules (the number of these modules depends on the problem complexity). These modules are connected to each

other by means of several elements that store information along with the programming functions. Classification processes including decision making, pattern recognition, and fault diagnosis are the most common tasks to which neural networks are applied.

Considerable attention to the application of neural networks for fault diagnosis has appeared in the literature. The practicality of neural networks for fault diagnosis in chemical engineering was demonstrated for the first time in the 1980s by researchers such as Venkatasubramanian and Chan [50] and Unger et al [51]. Later, the hierarchical neural network architecture, successful in the detection of multiple faults, was proposed by Watanabe et al. [52].

Back-propagation strategy, first described by Werbos in 1974, is the most conventional supervised learning technique for training neural networks. Back-propagation neural networks have been vastly investigated in engineering research in which problems of fault diagnosis are addressed. The idea of feature presentation, which has been demonstrated by Farell and Roat [53] and Tsai and Chang [54], is the foundation of the performance progress of the primary back-propagation neural networks in fault diagnosis applications. Recently, to overcome the slow convergence of the back-propagation algorithm a number of techniques such as the diagonal recurrent neural network have been proposed. Wang and He [55] introduced an adaptive dynamic back-propagation algorithm to determine the optimum number of the hidden layer neurons. They employed two diagonal recurrent neural networks to detect stator winding turn fault. One determines the fault intensity and the other is used to estimate the exact number of fault turns.

In addition to back-propagation, various network architectures have been studied in the fault diagnosis area. For example, Adaptive Resonance Theory 2 Neural Network (ART2 NN) is a self-organizing neural network structure, which is a prosperous methodology in fault diagnosis. Lee et al. [56] proposed an algorithm composed of three parts: parameter estimation, fault detection, and fault isolation. Once a fault is detected in the system, in order to isolate the occurred fault the estimated parameters are transmitted to the ART2 NN structure..

Wavelet Analysis

Wavelet analysis is a common methodology for analyzing localized variations of signal. In this method, to determine the dominant modes of variability and how those modes vary in time, a time series is decomposed into time–frequency space. The wavelet transform has been used for numerous studies, for example, Tafreshi et al. [57] used wavelet packet to recognize different conditions of one cylinder in a 12-cylinder engine. The combustion malfunctions in the cylinder were detected using the wavelet packet providing a useful data analysis structure for extracting features. Wang et al. [58] and Chen et al. [59] discuss the integration of ART networks with wavelets to develop fault diagnosis algorithms

3.3.2.2 Qualitative Model-free Methods

Qualitative model-free methodologies, which extract qualitative historical information, are studied in two major classes: a) expert systems and b) Qualitative Trend Analysis (QTA).

Fuzzy Approach

Zadeh [60] was the first to recognize the importance of the concept of the fuzzy theory. Rule-based feature extraction methodology has been broadly employed in expert systems for fault diagnosis applications. Important efforts to apply expert systems in fault diagnosis applications can be seen in the works of Hakami and Newborn [61] and Stewart [62]. The idea of using task framework in knowledge-based diagnostic systems was developed by Ramesh et al. [63]. Tarifa and Scenna [64] proposed a hybrid system that uses the combination of fuzzy logic and signed directed graphs (SDG). Scenna [65] discussed an expert system approach for fault diagnosis in batch processes. Leung and Romagnoli [66] described an implementation of a probabilistic model-based fault diagnosis expert system. Ghodsi and Sassani [67] demonstrated an adaptive fuzzy algorithm, which continuously adapts to variations in the input data. They demonstrated the efficiency of the structure in minimizing wood waste cutting process. Later, they improved the adaptive fuzzy algorithm using a recursive sub-algorithm to designate a preferred cut patterns among all possible patterns [68].

Qualitative Trend Analysis Approach

In process monitoring and supervisory control, qualitative trend analysis (QTA) is an important component, which is utilized to describe important events in a dynamic process to predict future condition and diagnose system faults. Even though the QTA is robust and accurate in system monitoring, its real-time application to very large-scale plants is prohibitive due to its computational complexity.

Initial formal framework for the representation of process trends can be found in Cheung and Stephanopoulos's work [69]. Vedam and Venkatasubramanian [70] proposed

an adaptive trend analysis framework based on the wavelet theory. Subsequently, they proposed a dyadic B-spline-based trend analysis algorithm achieving data compression by removing noise from the sensor data. Maurya et al. [71] resolved the shortcoming of the QTA in real-time applications by applying the QTA on the principal components rather than on the sensor data.

The mathematical model-based approach adopted in the present thesis falls into the observer category, which is described in Section 3.3.1.1. The approach is based on the Kalman Filter algorithm developed to monitor the highly non-linear dynamic systems.

3.4 Kalman Filtering in Fault Diagnosis

The Kalman Filter algorithm developed by R. Kalman is a recursive filter using noisy and even incomplete measurements to estimate the states of a linear system in the time domain. It is applied to the states of the discretised system to estimate the new states at each discrete time increment. Inputs of the algorithm are the system information and optionally some knowledge from the controls on the plant if it is known. The existence of two independent noises is considered; one perturbs the information from system (measurement noise) and the other is mixed with linear operator (process noise).

A general linear discrete-time system is represented by two equations; system equation:

$$x_{k+1} = Ax_k + Bu_k + w_k \tag{3.4}$$

and output equation:

$$y_k = Hx_k + v_k \tag{3.5}$$

where A is the state matrix, B is the input matrix, H is the output matrix, x is the state vector, y is the system output, u is the system input, w is the process noise and v is the measurement noise. Both process and measurement noises are assumed to have a mean of zero, and be Gaussian (normal distribution). There are process noise matrix Q and measurement noise matrix R, which are related to process noise vector w and measurement noise vector v, respectively. The noise matrices are the expected values (the sum of the probability of each possible consequence of the experiment multiplied by its value) of corresponding vectors described mathematically as

$$Q = E[ww^T] \tag{3.6}$$

and

$$R = E[vv^T] \tag{3.7}$$

where Q and R are the covariance matrices of the measurement noise and process noise, respectively. The noise level during measurements and the accuracy of sensors together with the modeling uncertainties (such as what is discussed in Section 2.4.1) are essential to derive the covariance noise matrices.

The Kalman filter performs the estimation in a predictor-corrector approach. Using the given system model, the *a priori* (predicted) state estimate vector at step k is defined from previous trajectory of x and calculated by the "Time-update" equation:

$$\hat{x}_k^- = A\hat{x}_{k-1} + Bu_k \tag{3.8}$$

where $\hat{x}_{k-1}$ is the previous time step *a posteriori* (corrected) state estimate vector and u_k is the known system input. The residual is defined as the difference between the measured and predicted output:

$$y_k - H\hat{x}_k^- \tag{3.9}$$

noting that when the Kalman filter is implemented in a real system, y_k is information from sensors, but in a simulation y_k is calculated from equation 3.5.

The *a posteriori* state estimate vector uses the information in the current observation and is calculated by the "Measurement-update" equation:

$$\hat{x}_k = \hat{x}_k^- + K_k(y_k - H\hat{x}_k^-) \tag{3.10}$$

where $\hat{x}_k^-$ is the *a priori* state estimate vector from Equation 3.8 and K_k is the Kalman gain. Note that if the residual ($y_k - H\hat{x}_k^-$) is zero, the *a priori* state estimate vector will equal the *a posteriori* state estimate vector. A function for the Kalman gain must be defined to minimize the *a priori* and *a posteriori* estimate errors and thus accurate estimation of the system states is achieved. The *a priori* and *a posteriori* estimate error covariances that we try to minimize are defined as:

$$P^- = E[(\hat{x}^- - x)(\hat{x}^- - x)^T] \tag{3.11}$$

and

$$P = E[(\hat{x} - x)(\hat{x} - x)^T] \tag{3.12}$$

respectively. Referring to [72] Chapter 4, the resulting function for the Kalman gain is

$$K_k = P_k^- H^T (HP_k^- H^T + R)^{-1} \tag{3.13}$$

and the minimized *a priori* estimate error covariance is found as

$$P_k^- = AP_{k-1}A^T + Q \tag{3.14}$$

and the minimized *a posteriori* estimate error covariance is

$$P_k = (I - K_k H)P_k^- \tag{3.15}$$

The Kalman algorithm should be initialized at first with the *a posterior* estimate error covariance and the state variable values. The recursive relations of the predictor-corrector structure for the Kalman filter can be presented by the block diagram as shown in Figure 3.2. This structure evolves into a computational scheme, which is run recursively in parallel with a sampled-data system to acquire the real-time state estimates. Sampled-data systems such as the one used in the present investigation and described in Chapter 2 are continuous-time dynamic systems controlled by digital devices.

Early attempts at the application of Kalman filter for fault diagnosis can be found in the works of Dalle Molle and Himmelblau [73] and Bergman and Astrom [74]. Tsuge et al. [75] introduced a hierarchical methodology consisting of the signed directed graph and the extended Kalman filter. Pirmoradi et al. [76, Chapter 23] investigated a Kalman filter methodology to track conditions of the spacecraft attitude control systems.

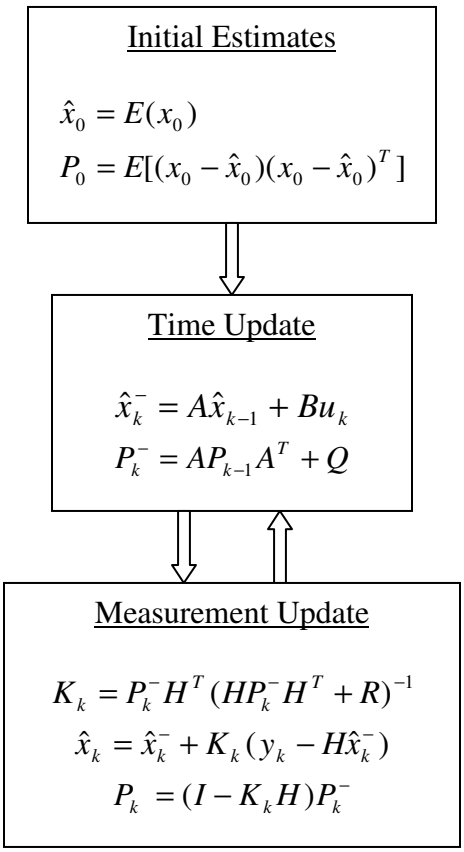

Figure 3.2: Kalman filter algorithm

Although the Kalman filter is a broadly used filtering strategy in system monitoring applications attributable to its optimality, robustness, and simplicity, the employment of the Kalman filter to non-linear systems is quite difficult. To overcome this shortcoming, the Extended Kalman Filter (EKF) [77] can be used instead. This method simply linearizes the non-linear state space model at each time step around the last states, then the "Time-update" and the "Measurement-update" phases are performed sequentially as shown in Figure 3.2. The EKF propagates the estimations through the first-order linearization; therefore it provides biased estimates when the system equations are highly non-linear. Although the EKF can be readily extended to incorporate higher

order terms, it leads to high computational costs. There are a number of weaknesses associated with the EKF algorithm such as [78]:

1. The EKF performance depends heavily on the time-step interval. For successive estimation it should be sufficiently small, especially for highly non-linear models, otherwise the linearization leads to unstable filter performance.
2. Providing Jacobian matrices makes the EKF not suitable for large dimension systems because of the calculation of the derivatives.
3. Since the EKF algorithm is based on linearization to propagate the covariance and mean of the system states, it gives unreliable estimates and is difficult to be tuned provided that the system is highly non-linear.

Although the EKF has been one of the most widely used algorithms for parameter estimation and tracking for forty years, it has led to a general agreement within the control community that the EKF is difficult to implement and because of the linearization error (as mentioned above) it is only reliable for systems, which are not highly non-linear on the time scale of the update intervals. In the next section, another non-linear transformation for the mean and covariance will be introduced to handle the linearization issue.

3.5 Unscented Kalman Filter

Generally, the basic difference between the EKF and the Unscented Kalman Filter (UKF) emerges from the manner in which the non-linear model states and parameters are approximated. The UKF introduced by Julier [79] employs the unscented transformation,

which is a non-linear transformation. In this algorithm, the state probability distribution is represented by a minimal set of data points, referred to as sampled sigma points.

3.5.1 Unscented Transformation

Julier and Uhlmann [77] calculated the mean and covariance by the use of a sampling approach, called the Unscented Transformation (UT), instead of an arbitrary non-linear function. Consider an *n*-element variable, $x \in \Re^n$, with known covariance, P_{xx}, and mean value, $\bar{x}$. To statistically approximate the mean and covariance of the non-linear transformation, $y = h(x)$ in which $y \in \Re^m$, a vector of $2n$ sigma points is formed according to the following:

$$\begin{aligned} \tilde{x}^{(i)} &= (\sqrt{nP})_i^T & i &= 1,...,n \\ \tilde{x}^{(n+i)} &= -(\sqrt{nP})_i^T & i &= 1,...,n \\ x^{(i)} &= \bar{x} + \tilde{x}^{(i)} & i &= 1,...,2n \end{aligned} \tag{3.16}$$

where $(\sqrt{nP})_i$ is the *i*th row of the $(\sqrt{nP})$; $(\sqrt{nP})$, which is called the matrix square root of *nP*, is defined as follows:

$$(\sqrt{nP})^T \sqrt{nP} = nP \tag{3.17}$$

Then the calculated sigma point vectors are simply propagated through the *h* function, which can be either linear or non-linear:

$$y^{(i)} = h(x^{(i)}) \qquad i = 1,...,2n \tag{3.18}$$

note that no linearization is applied for propagation. The estimated mean and covariance of *y* are determined as follows:

$$\bar{y}_u = \frac{1}{2n}\sum_{i=1}^{2n} y^{(i)}$$
$$P_u = \frac{1}{2n}\sum_{i=1}^{2n} (y^{(i)} - \bar{y}_u)(y^{(i)} - \bar{y}_u)^T \tag{3.19}$$

Simon in Chapter 14 of [80] investigated the UT. A typical problem was studied to make a comparison between UT and EKF performances. The non-linear transformations examined by Simon are as the following:

$$y_1 = r\cos\theta$$
$$y_2 = r\sin\theta \tag{3.20}$$

He calculated the covariance and mean of 300 stochastic points, which are dispersed uniformly in the ranges of $-0.01<r<0.01$ and $-0.35<\theta<0.35$ through both the UT and EKF. Then the unscented (from the UT) and linearized (from the EKF) results were compared with the exact (reference) data. Figure 3.3 depicts a summarized illustration of the approach for both UT and EKF along with the reference resolution.

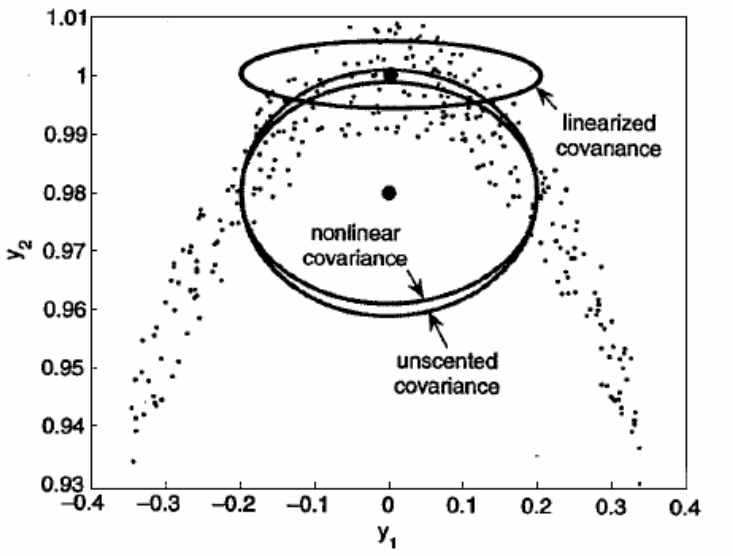

Figure 3.3: Compression of the UT and linear approximation
(From Optimal State Estimation, Dan Simon, Copyright © 2006, reprinted with permission of John Wiley & Sons, Inc.)

With the use of the UT algorithm the estimation of mean and covariance are closer to the real values and that holds because this approach leads to a third order accuracy for Gaussian inputs [81]. Contrarily, the linearization technique used in the EKF scheme results in the first order accuracy for similar inputs.

3.5.2 UKF Algorithm

The UKF algorithm is an extension of the UT to the recursive estimation in non-linear filtering problems. The UKF algorithm is summarized next [80]:

The following expressions form a general model of non-linear discrete-time systems to which the UKF may be applied at step k:

$$\begin{aligned} x_{k+1} &= f(x_k, u_k, t_k) + w_k \\ y_k &= h(x_k, t_k) + v_k \end{aligned} \tag{3.21}$$

in which f is the non-linear system function and h is the non-linear measurement function and the other parameters are the same as those defined in Section 3.4. The set of sigma points of the augmented state is constructed as:

$$\begin{aligned} \tilde{x}^{(i)} &= (\sqrt{nP_{k-1}})_i^T && i = 1,..., n \\ \tilde{x}^{(n+i)} &= -(\sqrt{nP}_{k-1})_i^T && i = 1,..., n \\ \hat{x}_{k-1}^{(i)} &= \hat{x}_{k-1} + \tilde{x}^{(i)} && i = 1,...,2n \end{aligned} \tag{3.22}$$

then the UKF can be proceeded by the predictor-corrector step in the Kalman filter algorithm. The *a priori* state estimate, $\hat{x}_k^-$, and its predicted error covariance, P_k^-, are calculated from the combination of the transformed sigma points as follows:

$$\hat{x}_k^{(i)} = f(\hat{x}_{k-1}^{(i)}, u_k, t_k) \tag{3.23}$$

$$\hat{x}_k^- = \frac{1}{2n}\sum_{i=1}^{2n}\hat{x}_k^{(i)} \tag{3.24}$$

$$P_k^- = \frac{1}{2n}\sum_{i=1}^{2n}(\hat{x}_k^{(i)} - \hat{x}_k^-)(\hat{x}_k^{(i)} - \hat{x}_k^-)^T + Q_{k-1} \tag{3.25}$$

Similarly the predicted observation vector $\hat{y}_k$ and its predicted covariance P_y are calculated as:

$$\hat{y}_k^{(i)} = h(\hat{x}_k^{(i)}, t_k) \tag{3.26}$$

$$\hat{y}_k = \frac{1}{2n}\sum_{i=1}^{2n}\hat{y}_k^{(i)} \tag{3.27}$$

$$P_y = \frac{1}{2n}\sum_{i=1}^{2n}(\hat{y}_k^{(i)} - \hat{y}_k)(\hat{y}_k^{(i)} - \hat{y}_k)^T + R_k \tag{3.28}$$

and the cross covariance matrix between $\hat{x}_k^-$ and $\hat{y}_k$ is obtained as:

$$P_{xy} = \frac{1}{2n}\sum_{i=1}^{2n}(\hat{x}_k^{(i)} - \hat{x}_k^-)(\hat{y}_k^{(i)} - \hat{y}_k)^T \tag{3.29}$$

The filter gain K_k, the updated state estimate $\hat{x}_k$, and the covariance P_k are computed as:

$$K_k = P_{xy}P_y^{-1} \tag{3.30}$$

$$\hat{x}_k = \hat{x}_k^- + K_k(y_k - \hat{y}_k) \tag{3.31}$$

$$P_k = P_k^- - K_k P_y K_k^T \tag{3.32}$$

The structure of the UKF can be presented by the schematic block diagram as shown in Figure 3.4.

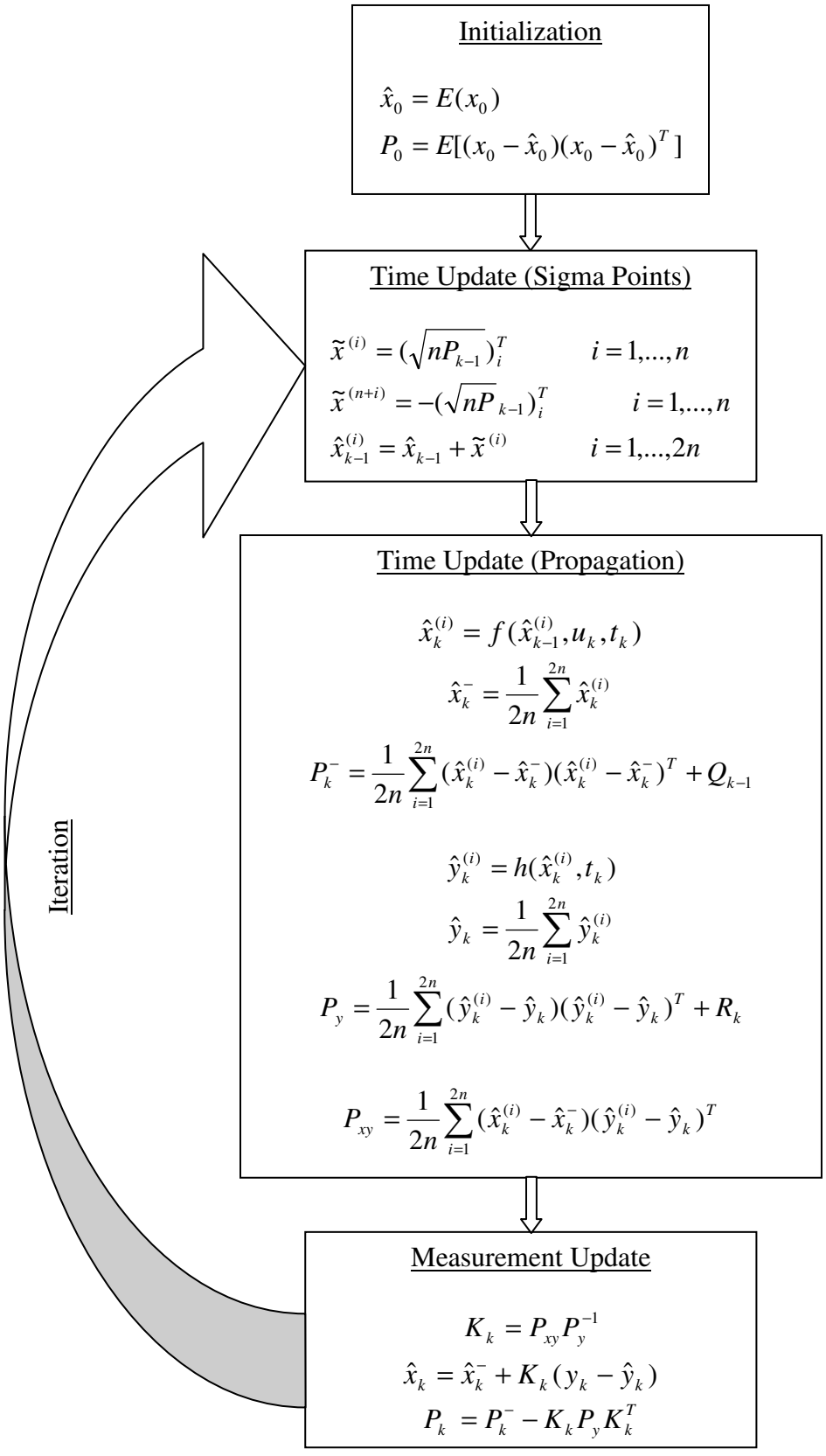

Figure 3.4: UKF structure block diagram

In contrast with the noise in real systems, both process and measurement noises are considered as additive and hence the explained UKF algorithm is not rigorous. Wan [82] augmented the noise onto the state vector as:

$$x_k^{(a)} = \begin{bmatrix} x_k \\ w_k \\ v_k \end{bmatrix} \tag{3.33}$$

then the augmented state $x_k^{(a)}$ is estimated. The initialization is as the following:

$$\hat{x}_0^a = \begin{bmatrix} E(x_0) \\ 0 \\ 0 \end{bmatrix} \tag{3.34}$$

$$P_0^a = \begin{bmatrix} E[(x_0 - \hat{x}_0)(x_0 - \hat{x}_0)^T] & 0 & 0 \\ 0 & Q_0 & 0 \\ 0 & 0 & R_0 \end{bmatrix} \tag{3.35}$$

Now the presented UKF can be used except that as we estimate the augmented mean and covariance, the terms Q_{k-1} and R_k should be removed.

3.6 UKF Application in the Hydraulic System

The UKF algorithm has been applied in non-linear control applications through the state estimation. The state space models are assumed known in these applications. In this section, we demonstrate the use of the UKF to the dynamic model explained in Chapter 2, and illustrate the results to show the performance of the developed algorithm.

3.6.1 The UKF Propagation

Since the UKF is a discrete-time algorithm and also in order to be compatible with real time digital computing, the state space equations should be discretised prior to using the UKF. Equation 3.36 shows the discretised state space model, which is derived by the use of Forward Difference method. Note that all parameters in this model are time invariant.

$$\begin{cases} x_1(k+1) = Tx_6(k) + x_1(k) \\ x_2(k+1) = \ldots \\ \begin{cases} \dfrac{T\beta}{V_0 + A_1(x_4(k) - X_{\min})}\left[C_d \omega x_1(k)\sqrt{\dfrac{2}{\rho}(x_2(k) - P_e)} - A_1 x_5(k)\right] + x_2(k) & x_1(k) > 0 \\ \dfrac{T\beta}{V_0 + A_1(x_4(k) - X_{\min})}\left[C_d \omega x_1(k)\sqrt{\dfrac{2}{\rho}(P_s - x_2(k))} - A_1 x_5(k)\right] + x_2(k) & x_1(k) < 0 \end{cases} \\ x_3(k+1) = \ldots \\ \begin{cases} \dfrac{T\beta}{V_0 + A_2(X_{\max} - x_4(k))}\left[C_d \omega x_1(k)\sqrt{\dfrac{2}{\rho}(P_s - x_3(k))} - A_2 x_5(k)\right] + x_3(k) & x_1(k) > 0 \\ \dfrac{T\beta}{V_0 + A_2(X_{\max} - x_4(k))}\left[C_d \omega x_1(k)\sqrt{\dfrac{2}{\rho}(x_3(k) - P_e)} - A_2 x_5(k)\right] + x_3(k) & x_1(k) < 0 \end{cases} \\ x_4(k+1) = Tx_5(k) + x_4(k) \\ x_5(k+1) = \dfrac{T}{M_a}(A_1 x_2(k) - A_2 x_3(k) - f_f(k) + F_{ext}) + x_5(k) \\ x_6(k+1) = T[-d_m \omega_n x_6(k) - \omega_n^2 x_1(k) + k_{sp} u(k+1)] + x_6(k) \end{cases} \tag{3.36}$$

in which T is the sampling time and k denotes the process step number. Due to the digital computing chrematistics of the computer used, the sampling time was chosen as 20 ms in this research. The discretised actuator friction is calculated from:

$$f_f(k) = \begin{cases} [f_{st} - (f_{st} - f_{sl})(1 - e^{-C|x_5(k)|})]sign(x_5(k)) + dx_5(k) & |x_5(k)| > v_0 \\ f_{st} & |x_5(k)| \le v_0 \end{cases} \tag{3.37}$$

Since the system has three outputs (measurements), two chamber pressures (x_2, x_3) along with the actuator displacement (x_4), the measurement matrix, which is linear here, can be written by inspection as:

$$H = \begin{bmatrix} 0 & 1 & 0 & 0 & 0 & 0 \\ 0 & 0 & 1 & 0 & 0 & 0 \\ 0 & 0 & 0 & 1 & 0 & 0 \end{bmatrix} \tag{3.38}$$

For the sake of simplicity, the noise characteristics of different states are assumed to be independent of each other. Therefore, the noise covariance matrices are diagonal. With reference to Figures 2.8 to 2.10, the MAEs between model output and test rig measurements are included in Table 3.1. Each MAE reflects the model uncertainty due the corresponding state. Therefore, the process noise matrix component in accord with the pressure in chamber 1 is 10^{10} Pa^2, the pressure in chamber 2 is 10^{10} Pa^2, and the actuator movement is 10^{-6} m^2.

Table 3.1: The MAEs of the pressures and actuator movement

State	Pressure in Chamber 1	Pressure in Chamber 2	Actuator Position
Model MAE	0.12 (MPa)	0.14 (MPa)	2.0 (mm)

Other components of Q matrix are determined regarding the physical attributes of the corresponding state. Then, these values are tuned to achieve the satisfactory UKF performance. The following matrix is defined as the process noise matrix in this system in each of the experiment:

$$Q = \begin{bmatrix} 10^{-20} & 0 & 0 & 0 & 0 & 0 \\ 0 & 10^{10} & 0 & 0 & 0 & 0 \\ 0 & 0 & 10^{10} & 0 & 0 & 0 \\ 0 & 0 & 0 & 10^{-6} & 0 & 0 \\ 0 & 0 & 0 & 0 & 10^{-6} & 0 \\ 0 & 0 & 0 & 0 & 0 & 10^{-20} \end{bmatrix} \tag{3.39}$$

in which all quantities are in the SI system.

The measurement noise matrix is defined regarding the accuracy of the sensors. The two msisensors® pressure transducers have the accuracy of 1.4×10^5 Pa and the accuracy of the Mitutoyo® position encoder is calculated as 3.5×10^{-6} m. Since there is no significant noise source near the set-up, it is assumed that the noise levels lie in the sensor accuracies. Therefore, the measurement noise matrix can be represented as the following in each of the experiment:

$$R = \begin{bmatrix} 10^{10} & 0 & 0 \\ 0 & 10^{10} & 0 \\ 0 & 0 & 10^{-11} \end{bmatrix} \tag{3.39}$$

in which all quantities are in the SI system.

The preceding matrices should be defined before the UKF algorithm can be built. Now the UKF must be initialized; regarding the UKF structure block diagram (Figure 3.4) $\hat{x}_0$ and P_0 should be defined. $\hat{x}_0$ is a 1×6 matrix whose second and third components, the chamber pressures, should be within the range of [P_e, P_s] and its fourth component, the actuator displacement, should be within the range of [X_{min} , X_{max}]. Generally, P_0 can be defined as a positive-definite matrix.

$$\begin{cases} \hat{x}_0 = \begin{bmatrix} 0 & 3.5\times10^6 & 3\times10^6 & 0.05 & 0 & 0 \end{bmatrix}^T \\ P_0 = diag\begin{bmatrix} 10^{-10} & 10^{10} & 10^{10} & 10^{-7} & 10^{-7} & 10^{-10} \end{bmatrix} \end{cases} \tag{3.40}$$

in which all quantities are in the SI system.

After setting the initial conditions as well as the covariance matrices the recursive part of the UKF algorithm can be performed in a series of steps. At first, *k* is unity and the sigma points are calculated. Following the UKF structure, these sigma points are propagated and the "measurement update" block is performed. Then to proceed in the recursive algorithm to the next time step, we return to sigma point calculations and *k* is incremented by one.

3.6.2 Simulation Results

After describing the UKF recursive algorithm as applied to the system, sample numerical simulations are run in this part. In order to simulate the measurement noise we call the Gaussian random number generator once every time-step interval and therefore the output is calculated via equation 3.5. By applying the UKF to the state space model a sequence of estimated state vectors is available and hereupon the estimation residual

vector can be computed by applying equation 3.9. Due to the measurement noise, R matrix, and the modeling uncertainties, Q matrix, the residual errors can not be ignored but still should remain at relatively low levels depending on the Q and R matrices' values.

To show the performance of the developed UKF, the residual errors in the state estimations of the system are presented in Figures 3.5 to 3.7. Figures 3.5 and 3.6 demonstrate the residual errors in the estimates of the chamber pressures. Figure 3.7 illustrates the residual error in the estimation of the actuator position.

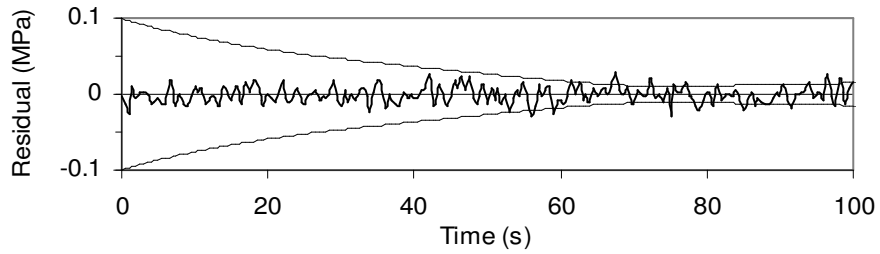

Figure 3.5: Estimation error of the pressure in chamber 1

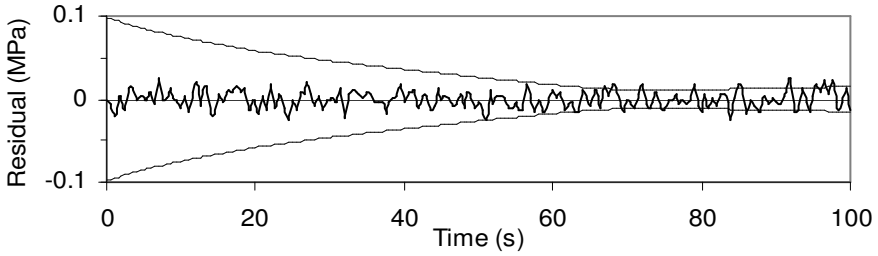

Figure 3.6: Estimation error of the pressure in chamber 2

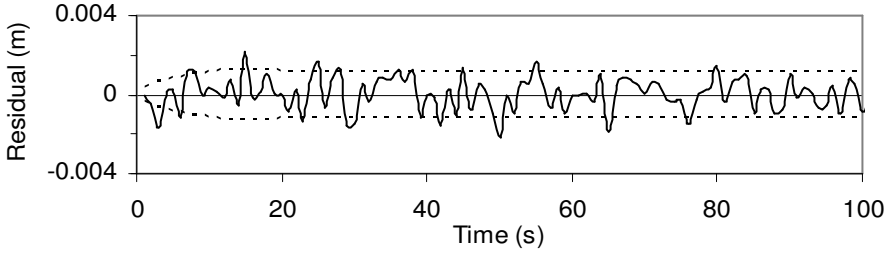

Figure 3.7: Actuator position estimation error

In the preceding graphs, dashed lines display the plus and minus values of the theoretical standard deviations of the corresponding measurements. Theoretically, the residual error results should fall within the $\pm\sigma$ bounds at least 68% of the time approximately. Accordingly, we can visually verify that the experimental and theoretical results appear to be in agreement. Note that in these simulations, the noise-added model represents the experimental data. This agreement should be held in order to show that the UKF algorithm is performing appropriately.

3.7 Concluding Remarks

In this chapter, fault diagnosis methods were surveyed and the overall structures of the Kalman filter and UKF schemes were described. The recursive part of the UKF consists of two phases, Time Update and Measurement Update. In "Time Update", the sigma points are calculated to be used in mean and covariance calculations, and then the *a priori* state estimates and covariances are obtained, while in "Measurement Update", the *a posteriori* state estimates and covariances are calculated. The purpose of this scheme is to estimate the system states and generate the residual errors, which is used in fault detection by threshold testing.

To verify the proposed UKF algorithm performance, it was applied to the state space model. The UKF used the information from the dynamic of the system along with the sensor measurements to predict future sensor outputs. The results showed that the difference between the actual and predicted states stayed in the acceptable bound. Therefore, the investigated UKF scheme is reliable to be employed in condition monitoring of the experimental set-up.

CHAPTER 4

Online Monitoring of the Hydraulic System

4.1 Introduction

Online condition monitoring through examining certain system state relationships and comparing the states with known nominal values is the most practical method to predict the occurred faults in hydraulic systems. This prediction increases the system efficiency by decreasing the chance of the further degradation beside the maintenance cost. To do so, an accurate state space model (as discussed in Chapters 2) along with a robust and reliable fault diagnosis methodology (as discussed in Chapters 3) is required.

In this chapter, the terminology used in [25] is employed to address the functions within the fault monitoring scheme:

Fault Detection

By the "Fault Detection" process, fault occurrence is determined along with its arising time.

Fault Diagnosis

By the "Fault Diagnosis" process, which includes fault detection, the size, location, kind and time of fault occurrence is determined.

Monitoring

By the "Monitoring" process, the conditions of the system are surveyed in real-time continuously.

In this chapter, the experimental results of artificially introduced faults into the hydraulic circuit are presented followed by the discussions pertaining to the fault diagnosis scheme performance.

4.2 Experimental Results and Discussion

Similar to the previous experiments and simulations, the sinusoidal signals are used as the position reference signals to control the test rig activities in this section. All the experiments are carried out under the UKF observation and a closed-loop control regulation. The reference signal is given as $r = 0.05 + 0.025\sin(0.4\pi t)$. Simulation results of previous chapters show that in the normal operational conditions the state space model follows the experimental test rig characteristics in a satisfactory precision and moreover the UKF scheme estimates the system states precisely. All proposed faults occur in the set-up approximately 50 seconds after the test starts and are kept until the end of the tests, which last 100 seconds. Note that faults exist in a multiple-fault environment but occur singly.

The matrices of the process noise, Q, measurement noise, R and initial covariance, P_0 along with the initial state vector are defined the same as what is derived in Section 3.6.1:

$$\begin{cases} \hat{x}_0 = \begin{bmatrix} 0 & 3.5\times10^6 & 3\times10^6 & 0.05 & 0 & 0 \end{bmatrix}^T \\ P_0 = diag\begin{bmatrix} 10^{-10} & 10^{10} & 10^{10} & 10^{-7} & 10^{-7} & 10^{-10} \end{bmatrix} \\ Q = diag\begin{bmatrix} 10^{-20} & 10^{10} & 10^{10} & 10^{-6} & 10^{-6} & 10^{-20} \end{bmatrix} \\ R = diag\begin{bmatrix} 10^{10} & 10^{10} & 10^{-11} \end{bmatrix} \end{cases} \tag{4.1}$$

The results of the experiments are reported in the following sections. The experiments were intended to diagnose the occurred faults in real-time operations. All five introduced faults are studied in two groups: leakage and load faults.

4.2.1 Leakage Faults

This section is developed to study the affects of leakages on the system. Therefore, different types of leakage faults in various levels are investigated.

4.2.1.1 Actuator External Leakage at Chamber 1

In this section, we introduce the fluid loss in the first chamber's connecting hoses. In real systems, this form of leakage may occur because of the poor pipe connections or hose ruptures. As a result of this fault, the pressure reduces in chamber 1 during an extraction stroke when this chamber is connected to the pressure supply line through the servo-valve.

The amount of the leakage is regulated manually by tuning the adjusting knob of the needle valve mounted on chamber 1. The bypass is illustrated in Figure 2.5. The

experiments are carried out for three different levels of the leakages as shown in Table 4.1.

Table 4.1: Multilevel leakage coefficients

Leakage level	**Effective Control Flow coefficient of the needle valve**
Low	C_v = 0.0143 (Valve open one turn)
Medium	C_v = 0.0612 (Valve open two turns)
High	C_v = 0.112 (Valve open three turns)

For brevity, since the system response is similar for all levels of leakages only the medium level is discussed in more detail here. Figure 4.1 shows the actuator displacement while medium level external leakage occurs at chamber 1. It can be verified visually that the actuator shifts slightly toward chamber 1 after the leakage occurs. This happens because the leakage at chamber 1 reduces the pressure in this chamber during the extracting period and as a result there is not sufficient power to identically push the piston toward chamber 2. Note that due to the closed-loop control, after about two cycles the piston stops shifting, but a bias error remains in the actuator referenced-movement.

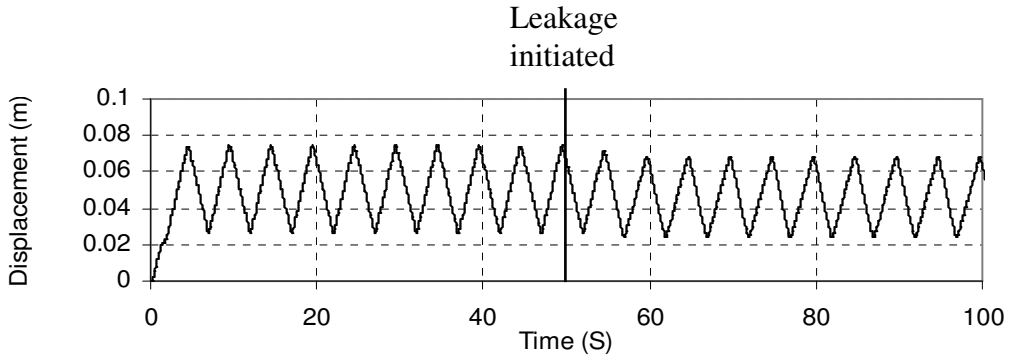

Figure 4.1: Actuator displacement while medium level leakage occurred in chamber 1

All three residual error signals due to the low level external leakage at chamber 1 are shown in Figure 4.2. It can also be observed visually that residual error of the corresponding state (pressure in chamber 1) increases slightly more than that of the pressure in chamber 2. This distinction is more obvious in the next two experiments in which medium and high level leakages are considered. The results are illustrated in Figures 4.3 and 4.4, respectively.

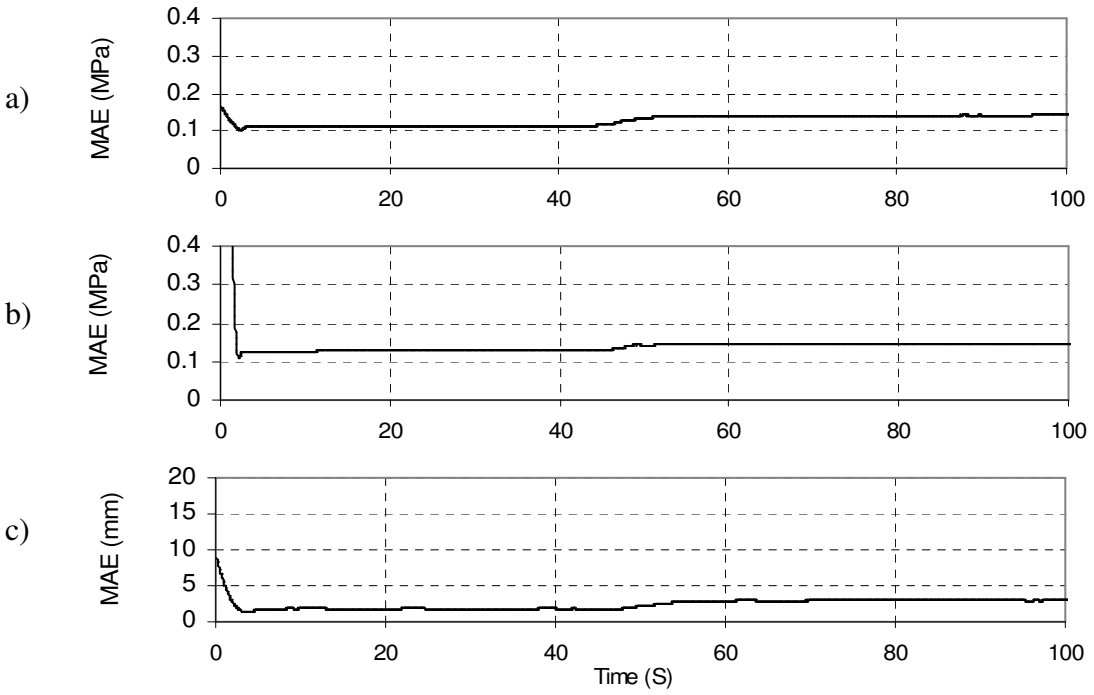

Figure 4.2: Low level leakage at chamber 1; (a) Residual errors of pressure in chamber 1, (b) pressure in chamber 2, and (c) actuator position

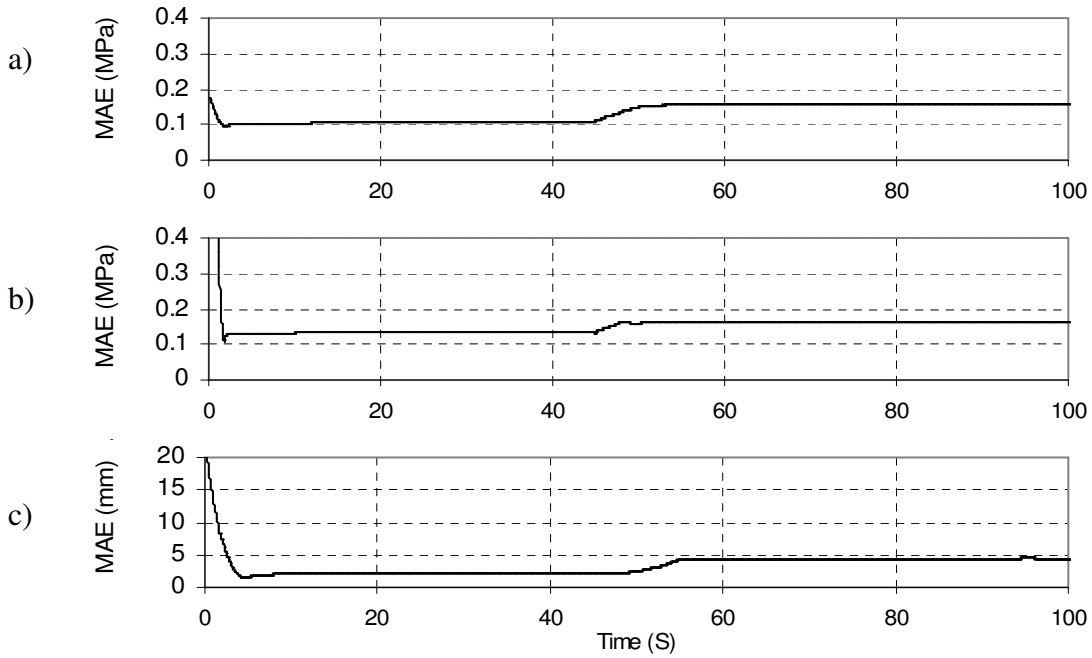

Figure 4.3: Medium level leakage at chamber 1; (a) Residual errors of pressure in chamber 1, (b) pressure in chamber 2, and (c) actuator position

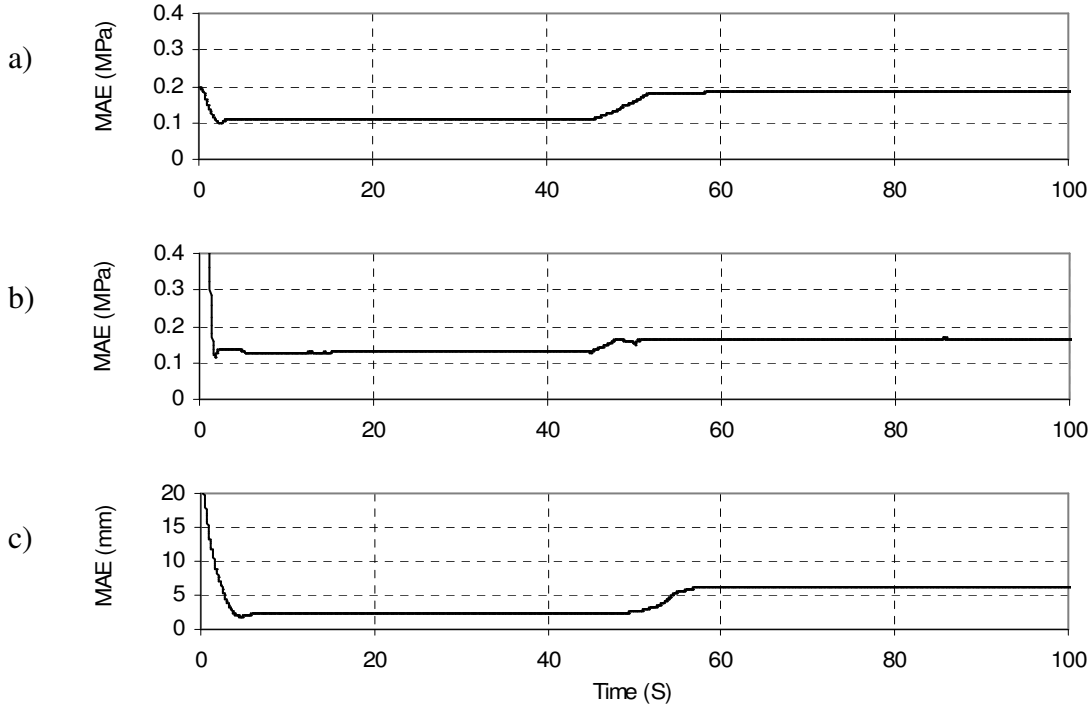

Figure 4.4: High level leakage at chamber 1; (a) Residual errors of pressure in chamber 1, (b) pressure in chamber 2, and (c) actuator position

The following table shows the corresponding variation of residual MAEs. It is intuitive that by opening of the needle valve, the leakage increases much more when the chamber 1 is activated, and therefore, the residual MAE increases more for higher level of leakage.

Table 4.2: Increase in MAEs due to the external leakage at chamber 1

Leakage level / **Measurand**	Low	Medium	High
Pressure in Chamber 1 (MPa)	0.026	0.05	0.073
Pressure in Chamber 2 (MPa)	0.016	0.026	0.034
Actuator Position (mm)	1.2	2.35	3.85

4.2.1.2 Actuator External Leakage at Chamber 2

The fluid loss in connecting hoses of chamber 2 is introduced in this section. As the system has same characteristics for different levels of leakages, the medium level of leakage is discussed in more detail here. Figure 4.5 illustrates the actuator displacement while medium level external leakage occurs in chamber 2. It is intuiuive that the actuator shifts toward chamber 2 accordingly after the occurrence of the leakage. The reason is that the leakage at chamber 2 reduces the pressure in this chamber during the retracting period and as a result there is not sufficient power to identically push the piston toward chamber 1. The same as previous section, after less than two cycles the piston stops shifting as a result of the closed-loop control, but a bias error remains. With reference to Figures 4.1 and 4.5, it does seem almost certain that the actuator malfunctions more

aggressively in the presence of the leakage at chamber 2 rather than that at chamber 1. This happens because the pressure is much higher in chamber 2 and therefore connecting this chamber to the tank causes more pressure loss, which leads to further defection in the system.

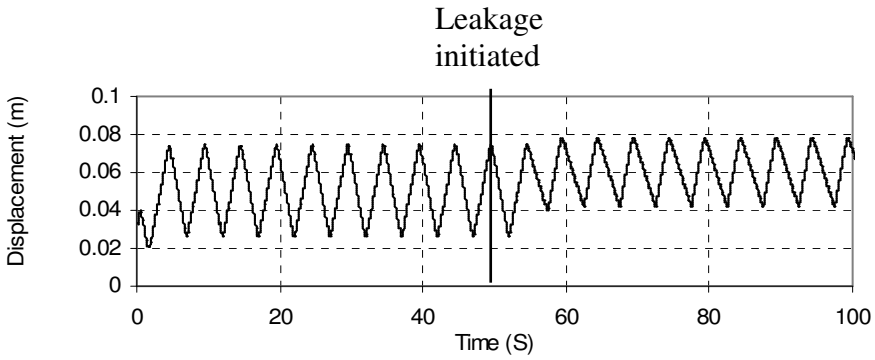

Figure 4.5: Actuator displacement while medium level leakage occurred in chamber 2

Figures 4.6 to 4.8 show the results of introducing leakage into chamber 2. Graphs indicate that the residual error of the pressure in chamber 2 increases much more than that in chamber 1. Similar to the previous section, these experiments are carried out considering three different leakage levels as shown in Table 4.1.

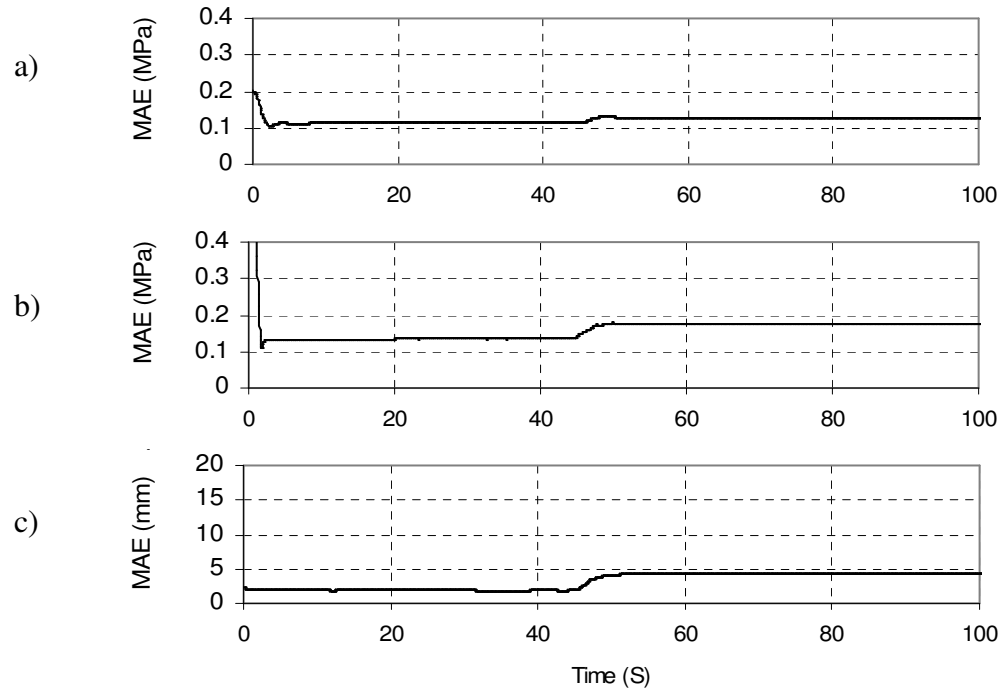

Figure 4.6: Low level leakage at chamber 2; (a) Residual errors of pressure in chamber 1, (b) pressure in chamber 2, and (c) actuator position

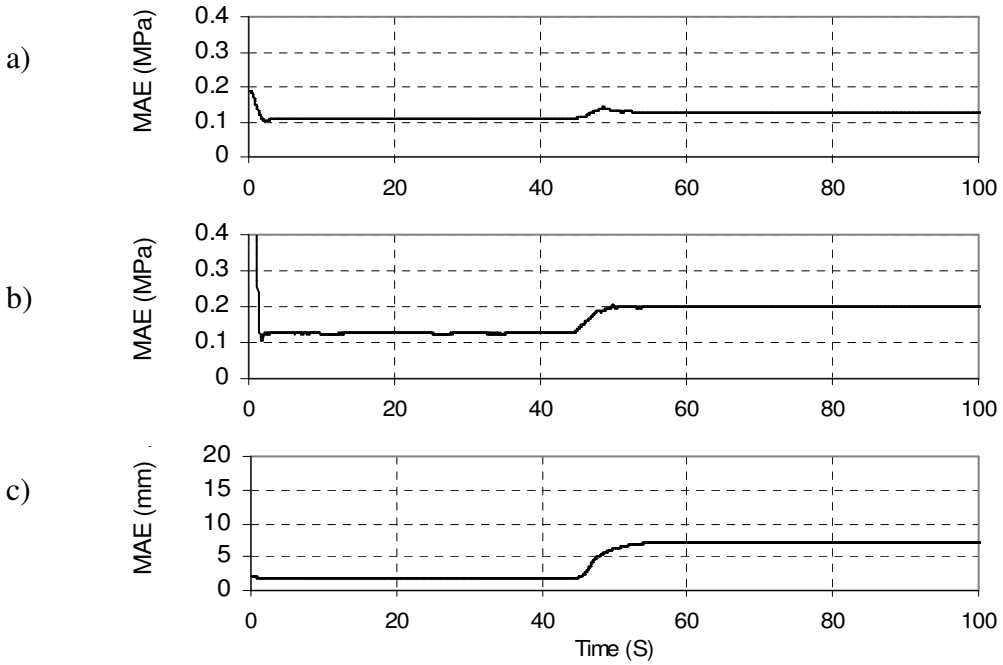

Figure 4.7: Medium level leakage at chamber 2; (a) Residual errors of pressure in chamber 1, (b) pressure in chamber 2, and (c) actuator position

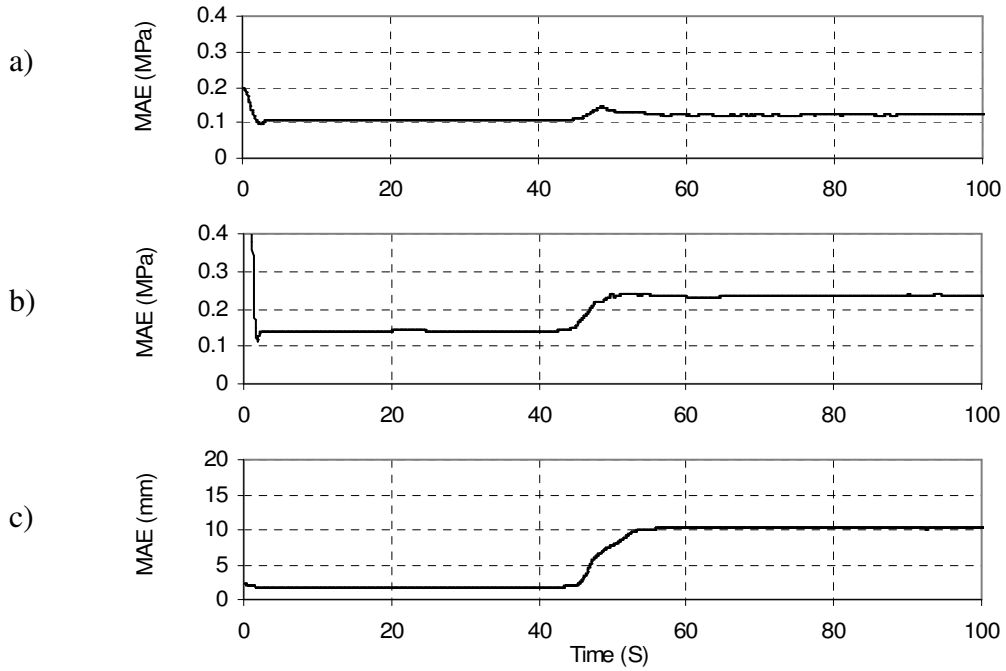

Figure 4.8: High level leakage at chamber 2; (a) Residual errors of pressure in chamber 1, (b) pressure in chamber 2, and (c) actuator position

What is noticeable in the results is that the residual MAE of the faulty chamber increases proportionally with the increase of the leakage. As expected, the residual MAE of the pressure in chamber 2 increases much more aggressively than that in chamber 1 as shown in Table 4.3.

Table 4.3: Increase in MAEs due to the external leakage at chamber 2

Leakage level / **Measurand**	Low	Medium	High
Pressure in Chamber 1 (MPa)	0.012	0.015	0.015
Pressure in Chamber 2 (MPa)	0.045	0.074	0.094
Actuator Position (mm)	2.75	5.4	8.5

4.2.1.3 Actuator Internal Leakage

In this section, experiments are carried out in order to assess the performance of the UKF algorithm in diagnosing of the actuator internal leakage. There are a number of potential causes that lead to internal leakage in a hydraulic cylinder, each of which may result in a set-up that fails to operate appropriately. For instance, if the cylinder's piston seal is impaired, fluid may leak internally between chambers. Furthermore, the internal leakage may occur as a result of the improper operation of a bypass valve. All of which may result in the differential force between the extension and retraction chambers be out of balance and hence the end-effector characteristics become unreliable.

In the experiments, the internal leakages are adjusted manually by tuning the knob of the cross-over needle valve shown in Figure 2.5. Tests are carried out for the same three leakage levels used earlier. Figure 4.9 illustrates the variation in actuator characteristic due to the medium level internal leakage occurrence. The point is that the actuator shifts toward the chamber with higher pressure (chamber 2). That is because the internal leakage decreases the pressure difference between two chambers and consequently the chamber with higher effective area (chamber 1) can apply more force to the piston.

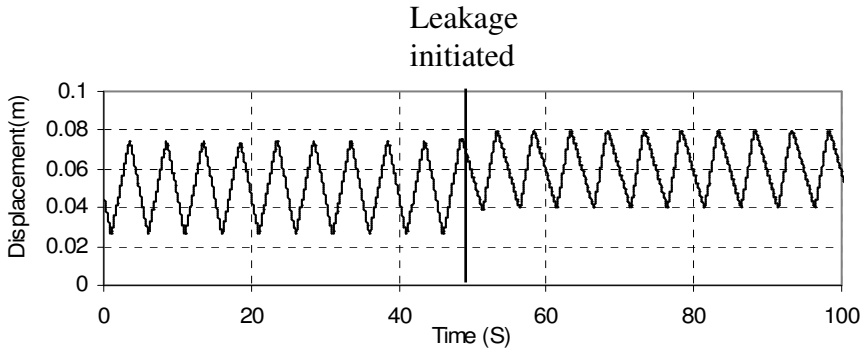

Figure 4.9: Actuator displacement while medium level internal leakage occurred

The residual errors due to the internal leakage are illustrated in Figures 4.10 to 4.12. However, the residual MAEs of all measurements increase, the increments in pressure MAEs are less than that in actuator displacement MAE. Moreover, these variations increase in amount for higher level of leakages.

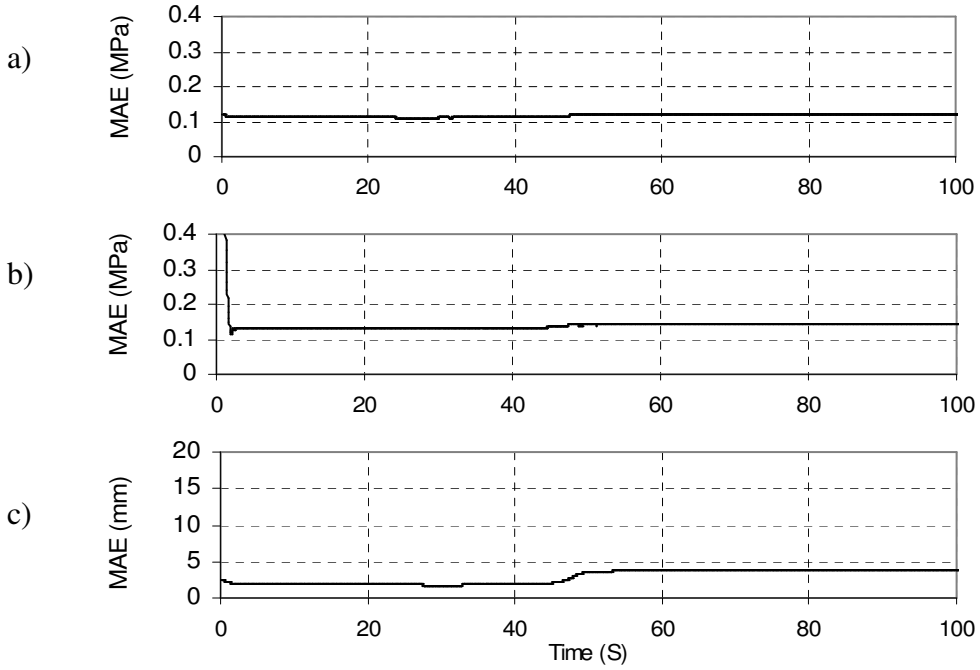

Figure 4.10: Low level internal leakage; (a) Residual errors of pressure in chamber 1, (b) pressure in chamber 2, and (c) actuator position

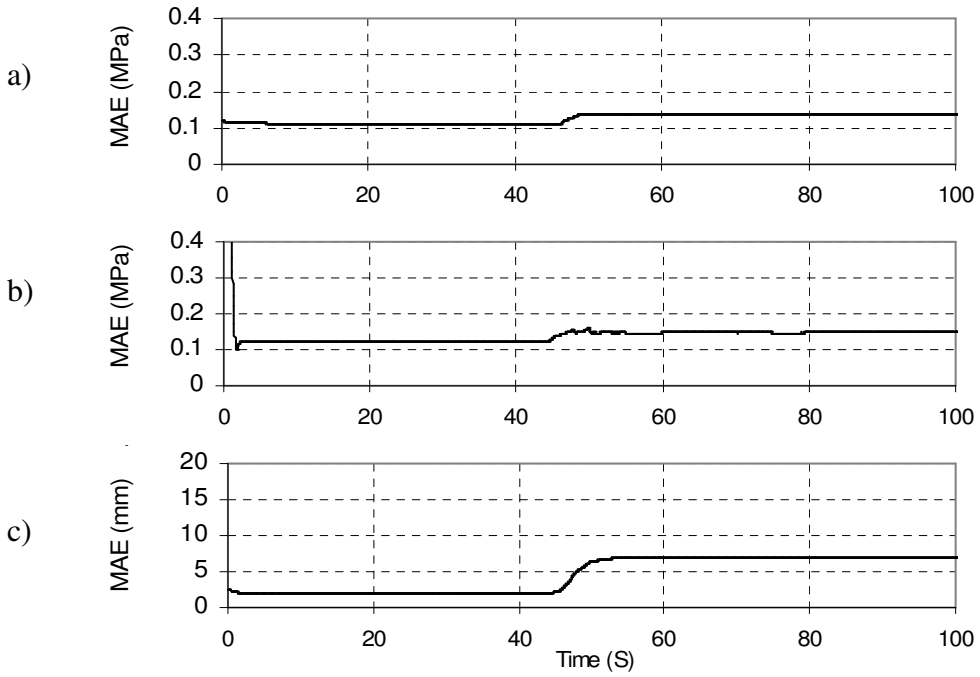

Figure 4.11: Medium level internal leakage; (a) Residual errors of pressure in chamber 1, (b) pressure in chamber 2, and (c) actuator position

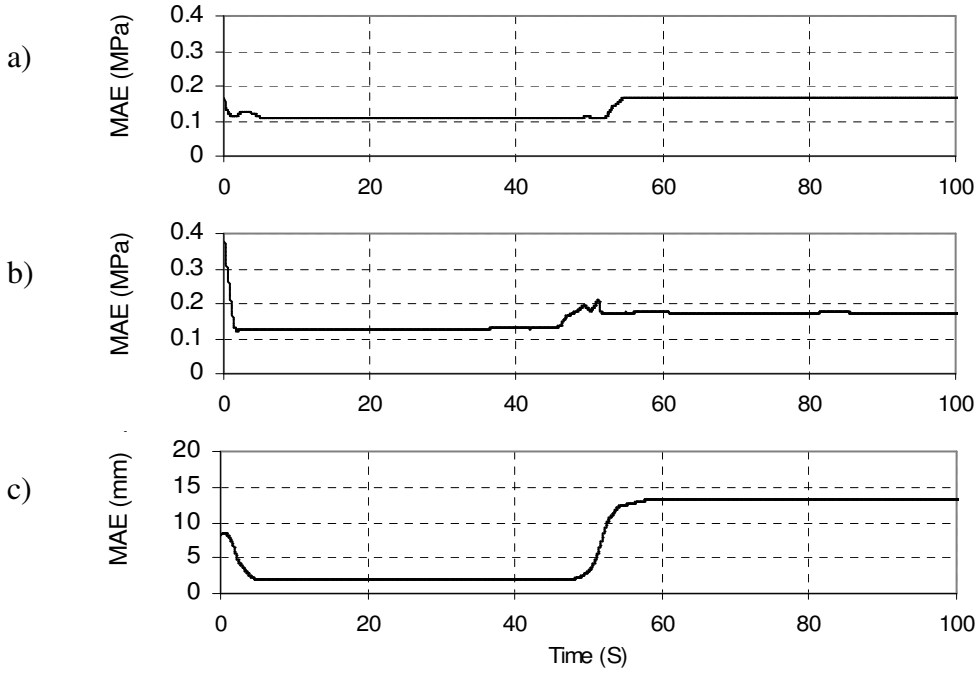

Figure 4.12: High level internal leakage; (a) Residual errors of pressure in chamber 1, (b) pressure in chamber 2, and (c) actuator position

Table 4.4 shows that as expected, the residual MAEs corresponding pressures are almost equal to each other.

Table 4.4: Increase in MAEs due to the internal leakage

Leakage level / Measurand	Low	Medium	High
Pressure in Chamber 1 (MPa)	0.01	0.028	0.057
Pressure in Chamber 2 (MPa)	0.008	0.025	0.046
Actuator Position (mm)	1.8	4.95	11.15

4.2.2 Load Faults

As opposed to the leakage faults, load faults are not quantified. Therefore, each set of test is carried out for a certain level of fault.

4.2.2.1 Dynamic friction load

This section is developed to study the affects of the dynamic friction load on the hydraulic system. This force is applied to the hydraulic actuator by means of the pneumatic cylinder as explained in Section 2.2. All experiments are carried out for the dynamic friction of 1162 N as the actuator is extracting and 1042 N as the actuator is retracting. These applied forces vary in amount because of utilizing the asymmetric pneumatic cylinder.

The following Figure shows the actuator displacement. There is no significant variation in the sinusoidal movement of the actuator after fault occurs. The reason is that

the controller compensates by inputting current with higher amplitude to the servo-valve, and therefore the capability of the actuator in making up for the dynamic friction load improves.

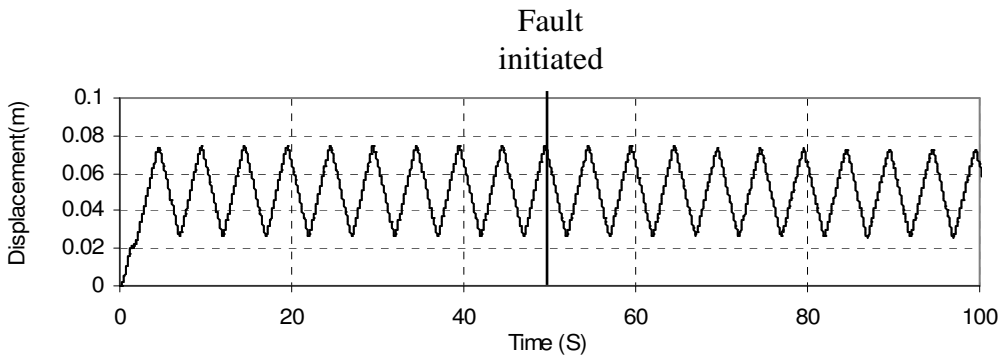

Figure 4.13: Actuator displacement while the dynamic friction load is applied

Figure 4.14 shows the residual error signals due to the dynamic friction load. It can be observed visually that residual error of the actuator position increases much more than that of the pressures in chambers 1 and 2.

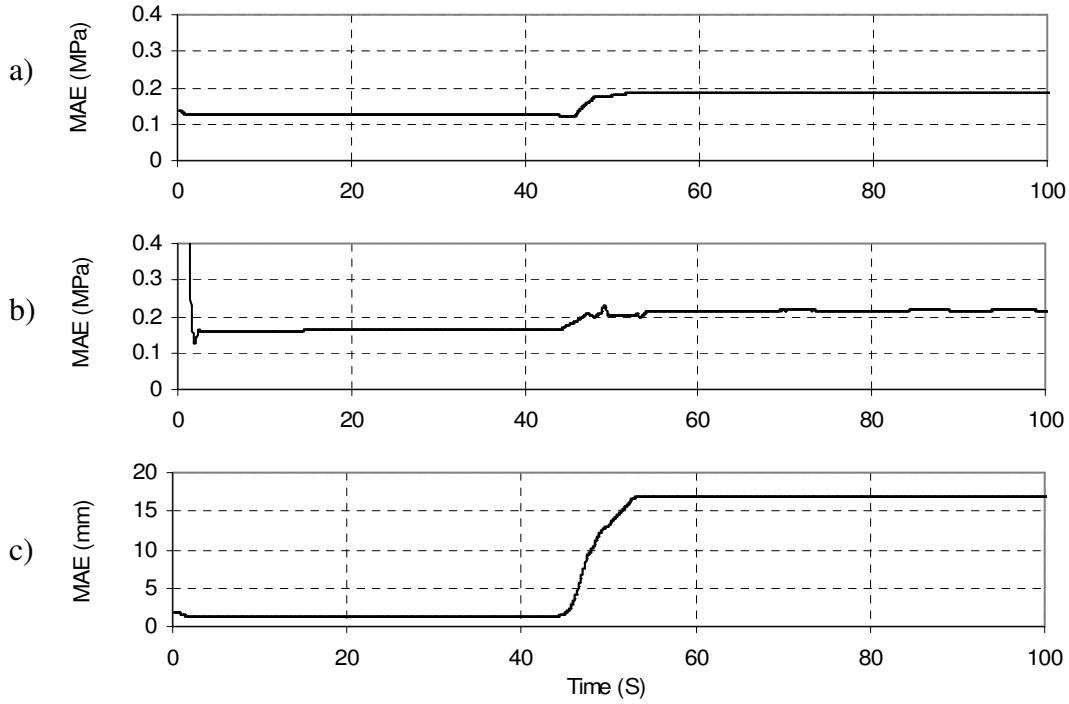

Figure 4.14: Dynamic friction load; (a) Residual errors of pressure in chamber 1, (b) pressure in chamber 2, and (c) actuator position

The following table presents the variation of residual MAEs. Both pressure residual errors increase equably.

Table 4.5: Increase in MAEs due to the dynamic friction load

Measurand	Pressure in Chamber 1 (MPa)	Pressure in Chamber 2 (MPa)	Actuator Position (mm)
Increase in MAE	0.061	0.05	13.0

4.2.2.2 Loss of Load

The goal of this section is to examine the system characteristics subject to loss of the load. This type of faults is mostly related to the industrial robotics and crane machinery. In this experiment two weights are disconnected from the actuator simultaneously. Similar to the previous section result, removing the load does not cause significant disturbance to the end-effector movement as shown in the following figure.

With a comparison between the actuator characteristics in this and previous experiments, it can be observed that the actuator movement diverges from the reference signal by occurrence of any leakage fault. Although, it follows the reference signal satisfactorily by occurrence of faults regarding the load. The reason is that by applying any disturbance on the healthy system the regulator starts compensating via the current input to the servo-valve. In leakage scenarios the servo-valve increases the pressures of the corresponding chambers. Since the leakage is proportional to the pressure difference, the amount of the leakage intensifies, but it is not a case of load faults. The following equation expresses the leakage through the needle valve:

$$q = C_v x_v \sqrt{\Delta p} \tag{4.2}$$

in which C_v is the flow coefficient, x_v is the valve spool position, and Δp shows the pressure difference between valve ports.

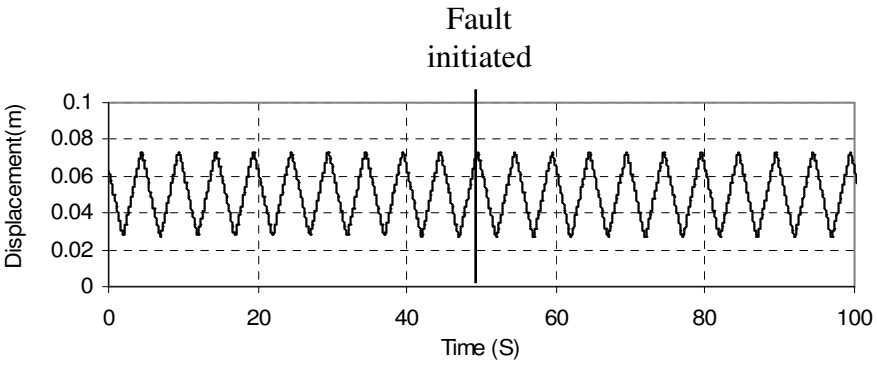

Figure 4.15: Actuator displacement while the load is removed

Experimental results are illustrated in Figure 4.16. All residual MAEs increase just as the fault occurs and also this variation for actuator displacement residual is much more than that for pressure residuals.

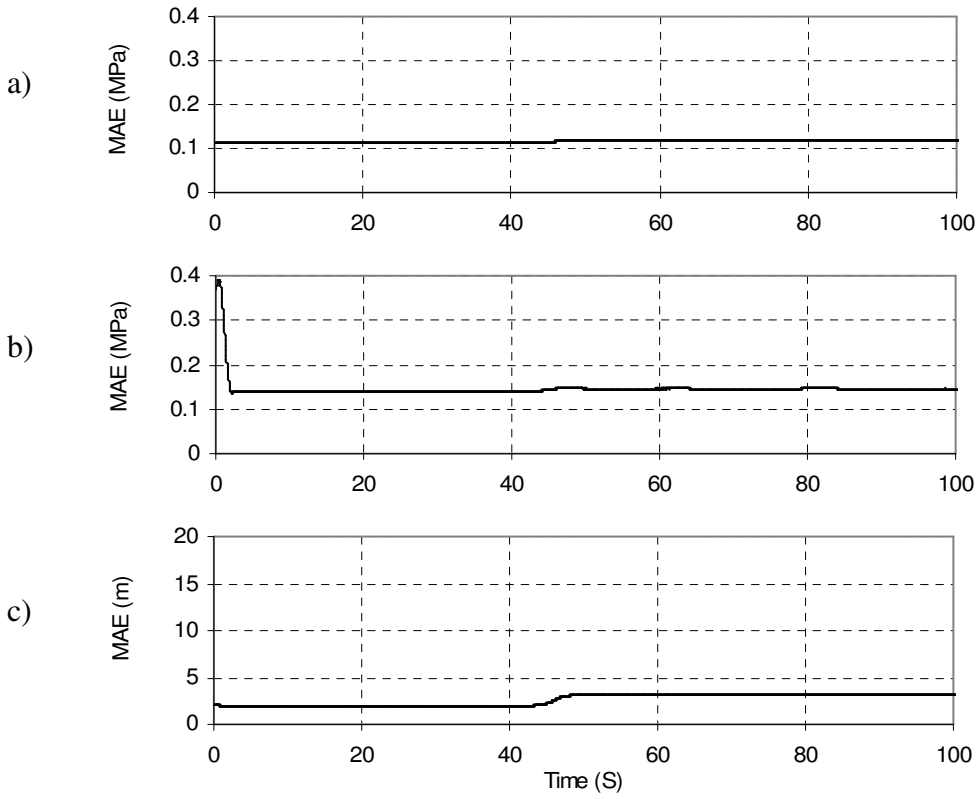

Figure 4.16: Load lost; (a) Residual errors of pressure in chamber 1, (b) pressure in chamber 2, and (c) actuator position

Corresponding variation of the residuals are shown in Table 4.6. The same as previous section, pressure residual errors increase equably.

Table 4.6: Increase in MAEs due to the load lost

Measurand	Pressure in Chamber 1 (MPa)	Pressure in Chamber 2 (MPa)	Actuator Position (mm)
Increase in MAE	0.007	0.006	1.3

4.3 Fault Diagnosis and Discussion

The performance of the designed fault monitoring scheme in fault detection has been discussed in Section 4.2. The fault can be diagnosed reliably in a case that fault signatures are distinguishable satisfactorily. Table 4.7 provides the variations of residual MAEs of the three measurements corresponding to all five studied faults.

In order to diagnose the occurred fault, there are three criteria that should be concerned; residual MAEs, chamber pressures, and actuator characteristics. The influences of each fault on the system, which lead to the fault diagnosis, are described individually.

4.3.1 Leakage at Chamber 1

In a case that the residual MAE of pressure in chamber 1 increases almost to twice or more than that in chamber 2, it can be concluded that external leakage occurs at chamber 1 regardless of any other criterion variation. Since the residual errors increase proportional to the amount of the leakage at chamber 1, the intensity of the external leakage can also be estimated by observing the amounts of the residual error increments.

Table 4.7: Increase in MAEs due to the occurred fault

Measurand / **Fault**	Pressure in Chamber 1 (MPa)	Pressure in Chamber 2 (MPa)	Actuator Position (mm)
Leakage at Chamber 1 (Low)	0.026	0.016	1.2
Leakage at Chamber 2 (Low)	0.012	0.045	2.75
Internal Leakage (Low)	0.01	0.008	1.8
Leakage at Chamber 1 (Medium)	0.05	0.026	2.35
Leakage at Chamber 2 (Medium)	0.015	0.074	5.4
Internal Leakage (Medium)	0.028	0.025	4.95
Leakage at Chamber 1 (High)	0.073	0.034	3.85
Leakage at Chamber 2 (High)	0.015	0.094	8.5
Internal Leakage (High)	0.057	0.046	11.15
Dynamic friction load	0.61	0.5	15.5
Load Rupture	0.007	0.006	1.3

4.3.2 Leakage at Chamber 2

The difference between the pressure residual error increments is much higher in the presence of leakage at chamber 2 rather than that at chamber 1 for a certain leakage level. As an instance for medium-level leakage occurrence in chamber 1, the residual MAE of pressure in chamber 1 increases 24 kPa more than that in chamber 2, but for a medium-level leakage at chamber 2 the residual MAE difference between chamber 1 and chamber 2 is 59 kPa. However, still we follow the regulation regarding the leakage at chamber 1. This imitation is decided for the sake of simplicity of the real-time practical fault monitoring scheme.

Therefore, in a case that the residual MAE of pressure in chamber 2 increases almost to twice or more than that in chamber 1, it can be concluded that external leakage occurs at chamber 2 regardless of any other criterion variation. Since the residual errors increase proportional to the amount of the leakage at chamber 2, the intensity of the external leakage can also be estimated by observing the amounts of the residual error increments.

4.3.3 Dynamic Friction Load

It can be observed that by occurrence of either internal leakage or load faults all residual MAEs grow, however, as opposed to the presence of external leakage, residual errors of pressure in chamber 1 and chamber 2 increase almost identically. To distinguish the dynamic friction load, it is essential to consider the characteristics of pressures and actuator movement. Figure 4.17 shows the pressure attributes as the dynamic friction load takes place.

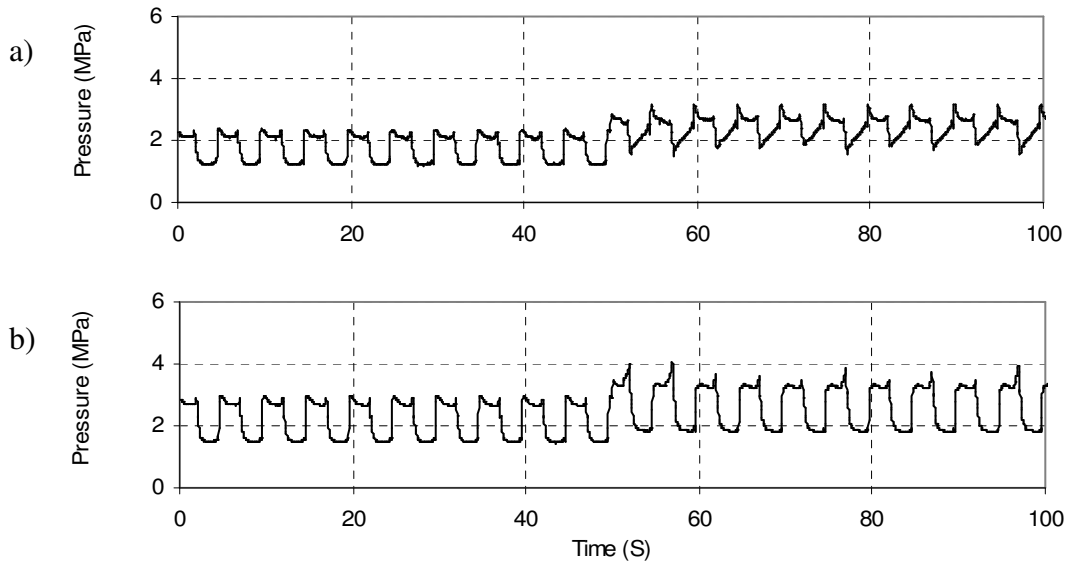

Figure 4.17: Pressure characteristics in dynamic friction load occurrence; (a) pressure in chamber 1, and (b) pressure in chamber 2

It can be observed that to compensate the external force, higher pressures are applied on the actuator, which leads to the agreement between the end-effector movement and the reference signal (as illustrated in Figure 4.13).

In summary, when the dynamic friction load fault occurs, the pressure residual errors grow almost equably along with the increase in the actuator displacement residual error. Moreover, pressure transducers measure higher pressures at both chambers as the opposite of the position encoder, which shows no variation in the actuator movement.

4.3.4 Loss of Load

Again, all three criteria should be considered to diagnose the load disconnection. The residual error increment trends are consistent with those of the dynamic friction load experiment. As illustrated in Figure 4.15 there is no significant variation in the actuator referenced-movement while the load is removed. To study the pressure characteristics, pressure transducer signals are shown in the following figures.

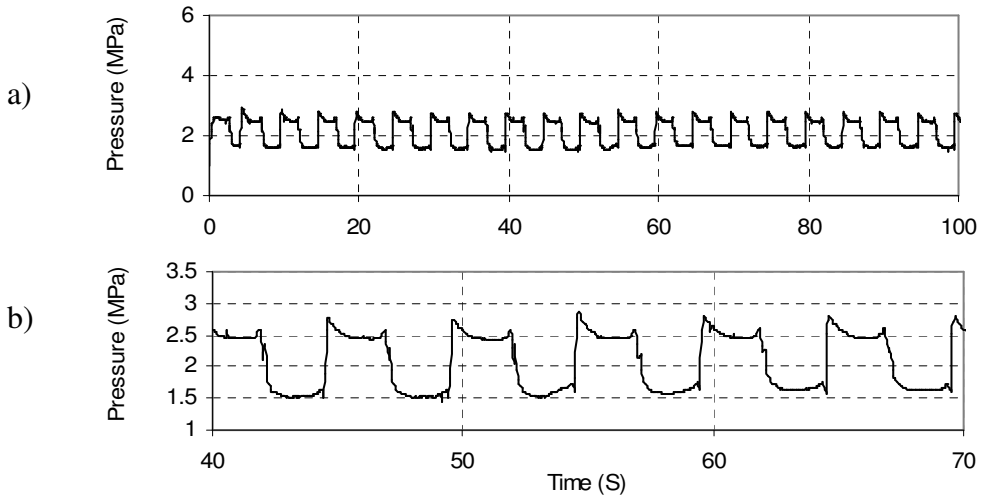

Figure 4.18: (a) Pressure in chamber 1 while the load is removed and (b) the close-up plot

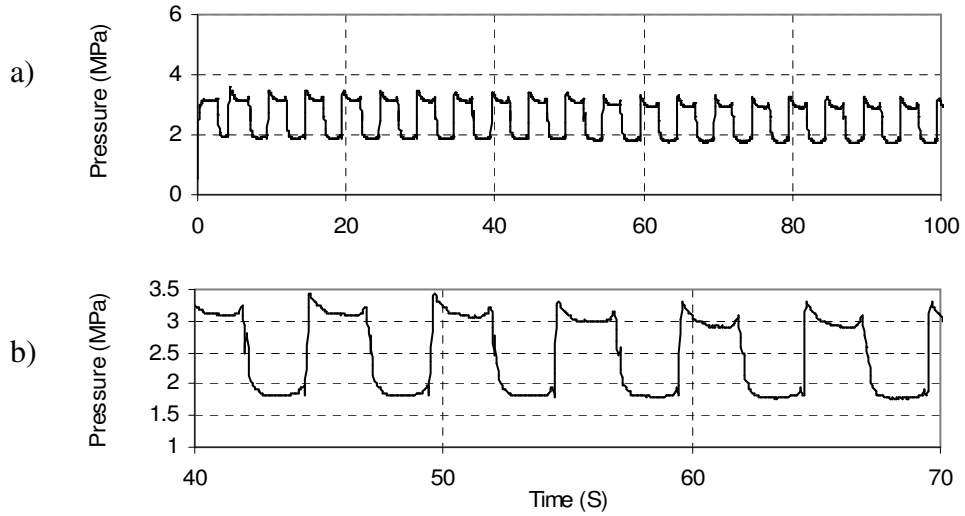

Figure 4.19: (a) Pressure in chamber 2 while the load is removed and (b) the close-up plot

The close-up plots show the pressure variations better at the time of load disconnection, from which it can be seen that pressure in chamber 1 increases slightly while the pressure in chamber 2 decreases a little. This happens because of the asymmetry in the load attached to the actuator as discussed in Section 2.2. In scenarios in which symmetric loads are applied to the actuator, due to the acceleration issue, by

removing the load the pressure transducers show less pressures in compare with the time that the fault is not introduced to the system.

In summary, when the load is disconnected, the pressure residual errors grow almost equably along with the increase in the actuator displacement residual error. Moreover, at least one of the pressures decreases in amount while the position encoder displays no variation in actuator referenced-movement.

4.3.5 Internal Leakage

By introducing the internal leakage to the actuation system the most significant characteristic variation pertains to the actuator movement as shown in Figure 4.9. This variation makes the internal leakage fault distinguishable from faults related to the load. However, the pressures in chambers decrease in this experiment. Figure 4.20 illustrates the pressures while the high level of internal leakage occurs in the system.

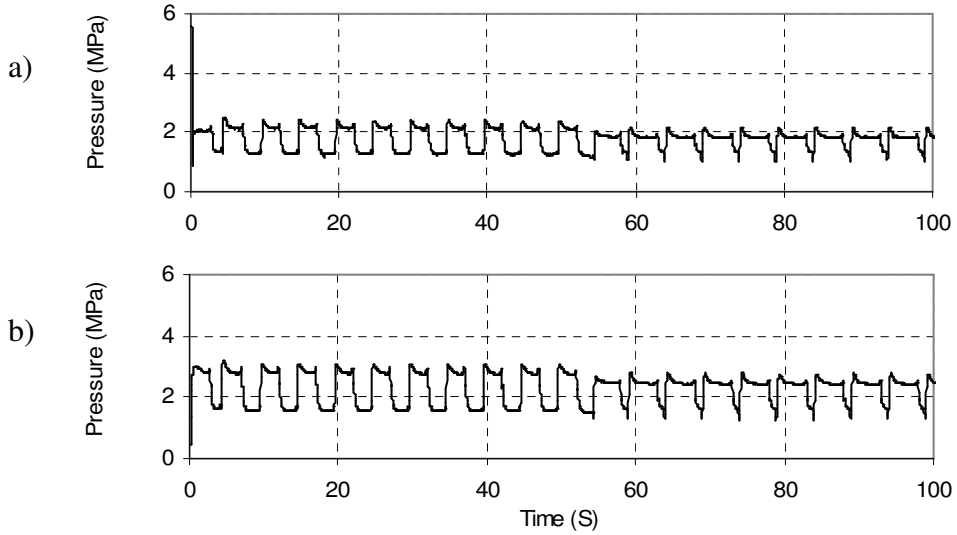

Figure 4.20: Pressure characteristics in internal leakage occurrence; (a) pressure in chamber 1, and (b) pressure in chamber 2

Pressures reduce because both chambers are connected to the tank continuously after the internal leakage is introduced. For instance, chamber 1 is connected to the return line directly during the retraction period while it is connected to the return line through the needle valve, which emulates the internal leakage, and chamber 2 during the extraction period.

In summary, when the internal leakage occurs, the pressure residual errors grow almost equably along with the increase in the actuator displacement residual error. Moreover, pressure transducers show decreases in pressures. Another point that should be notified is the actuator movement variation from the reference signal. Since the residual errors increase proportional to the amount of the leakage as it can be observed from Table 4.7, the intensity of the cross-port leakage can also be estimated by observing the amounts of the residual error increments.

CHAPTER 5

Conclusion

5.1 Summary

The goal of this research was to develop an on-line condition monitoring technique based on the Unscented Kalman Filter (UKF). This scheme was applied to a hydraulic test rig to diagnose artificially induced faults. Since the UKF requires an accurate model of the system to give good estimation of the system states, the set-up was inspected carefully to derive its state space model.

First, the investigated test rig configuration was explained with the aid of pictures and schematic diagrams. Two subsystems, pneumatic and hydraulic, together with their essential components were described in detail. All five potential faults, which were emulated by the current scheme, were discussed, namely:

1, 2. External leakages at both hydraulic cylinder chambers

3. Dynamic friction load

4. Sudden loss of load

5. Leakage inside of the hydraulic cylinder

Then, the linear time-invariant state space model corresponding to the set-up was derived. Six state variables characterized the system: the servo-valve spool displacement and velocity, the hydraulic cylinder chamber pressures, and the actuator displacement and velocity. This mathematical model was further elaborated with the details of the various governing equations, function modeling, and all related parameters. A number of experiments were carried out to determine the parameters, which were not measurable directly such as the parameters of the actuator friction model. Then, to validate the state space model, a sinusoidal position reference signal was applied to the closed-loop system. The results verified that the system model characteristics satisfactorily converged to the corresponding set-up features as it operated in normal conditions.

Fault detection and diagnosis techniques were explained, and a number of valuable previous works were outlined for each of the methodologies. The Kalman filter and EKF algorithms were studied in more detail, and their advantages and disadvantages when applied to dynamic systems were discussed. Then, the UKF was introduced and its capabilities in handling the highly non-linear systems were described. Its satisfactory performance in state estimation was tested on the model of the set-up. The measurement data were generated by adding white noise to the output of the mathematical model of the hydraulic test rig. The estimation results of three states, actuator displacement and chamber pressures, were compared with the measurement data to generate residual errors. Since all the errors were satisfactorily within the acceptable bandwidth, it was concluded that the UKF methodology was reliable to be employed in condition monitoring of the experimental set-up.

The developed UKF-based fault monitoring scheme was tested on the physical system while different fault scenarios were singly introduced to the system. Again, a sinusoidal reference signal was used for the actuator displacement. The fault diagnosis scheme estimated the system states and generated residual errors in real time. To diagnose the occurred fault, three criteria, residual MAEs, chamber pressures, and actuator characteristics, were considered. Based on the presented experimental results and discussions, the proposed scheme could reliably diagnose the occurred faults. Also, for each leakage scenario, three levels of leakages were introduced to the test rig. However, it was impracticable to evaluate quantity of the leakage from residual errors, the proposed algorithm can be employed to qualitatively assess the leakage level.

5.2 Contributions

This thesis consists of a number of contributions, which have been made to both fields of hydraulics and fault diagnosis. The major contributions of this thesis are outlined below:

- A fully operational hydraulic test rig capable of emulating faults was constructed.
- A novel UKF application in hydraulic systems for on-line diagnosis of faults was proposed. This structure accepted raw sensor data as input and automatically generated fault symptoms.
- Five of the most common faults in industrial hydraulic systems were investigated. Two faults were related to the load and three were pertinent to

the external leakage on either side and internal to the actuator. The leakage faults were quantified and the proposed fault monitoring scheme was successful in indicating the leakage fault level.

- A comprehensive mathematical model for accurate simulation of a servo-actuator system was developed and validated using the experimental data. The asymmetry of the system (the asymmetric load was carried by the asymmetric cylinder) was the major challenging aspect in this test rig. The model calculations converged to the sensor data with an MAE within 10% of the actual measurements.

5.3 Suggestions for Future Works

Model-based fault diagnosis for an uncertain non-linear system is an extremely rich area for research both in terms of theoretical problems and practical implementation issues. There are many ways to improve the proposed technique or introduce new methods. In future works, the proposed strategy can be extended in the following direction:

- The state space model acquired for fault monitoring can be extended to incorporate other hydraulic and even pneumatic components. To do so, it is required to obtain good representative mathematical models and appropriate estimation for their parameters. As a result, the system states may be predicted more accurately, which makes the system more reliable.

- An expert system can diagnose the occurred fault by considering the UKF estimations, residual errors and sensor signals, in real-time. Designing and implementing a graphical user interface to show decisions of the expert system is also desirable.

- More common faults can be introduced to the system to examine the effectiveness of the proposed condition monitoring scheme in diagnosing them.

- Inducing and diagnosing multiple faults can also be investigated to improve the applicability and utility of the monitoring system.

References

[1] Ogata, k., 2006, "Modern Control Engineering," Pearson.

[2] Merritt, H.E., 1967, "Hydraulic Control Systems," John Wiley & Sons Inc.

[3] Sassani, F., Lawrence, P. D., and Khoshzaban, M., 1998, "On-Line Monitoring a Hydraulic Arm Using Physical Parameter Tracking," World Automation Congress (WAC'98), Anchorage, in: Intelligent Automation and Control - Recent Trends in Development and Applications, vol. 6 pp: ISIAC 117.1 - ISIAC 117.9

[4] Alleyne, A., and Rui, L., 1999, "On the Limitations of Force Tracking Control for Hydraulic Servosystems," Journal of Dynamic Systems, Measurement, and Control, 121(2), pp. 184-190.

[5] Plummer, A., and Vaughan, N., 1996, "Robust Adaptive Control for Hydraulic Servosystems," Journal of Dynamic Systems, Measurement, and Control, 118(2), pp. 237-244.

[6] Gertler, J.J., 1998, "Fault Detection and Diagnosis in Engineering Systems," Marcel Dekker.

[7] Dutton, K., and Groves, C., 1996, "Self-Tuning Control of a Cold Mill Automatic Gauge Control System," International Journal of Control, 65(4), pp. 573-588.

[8] Popescu, M., Arsenie, D., and Vlase, P., 2004, "Applied Hydraulic Transients for Hydropower Plants and Pumping Stations," Taylor & Francis.

[9] Chen, W., and Saif, M., 2006, "An Iterative Learning Observer for Fault Detection and Accommodation in Nonlinear Time-Delay Systems," International Journal of Robust Nonlinear Control, 16(1), pp. 1-19.

[10] Zavarehi, M. K., Lawrence, P. D., and Sassani, F., 1999, "Nonlinear Modeling and Validation of Solenoid-Controlled Pilot-Operated Servovalves," IEEE/ASME Transactions on mechatronics, 4(3), pp. 324-334.

[11] Niksefat, N., and Sepehri, N., 2002, "A QFT Fault-Tolerant Control for Electrohydraulic Positioning Systems," IEEE Transactions on Control Systems Technology, 10(4), pp. 626-632.

[12] Crowther, W. J., Edge, K. A., Burrows, C. R., 1998, "Fault Diagnosis of a Hydraulic Actuator Circuit using Neural Networks—An Output Vector Space Classification Approach," Proceedings of the Institution of Mechanical Engineers, Part I: Journal of Systems and Control Engineering, 212(1), pp. 57-68.

[13] Heron, R., and Huges, M., 1986, "A Contaminant Monitor for Fluid Power Applications," International Conference on Condition Monitoring, UK, pp. 57-71.

[14] An, L., and Sepehri, N., 2005, "Hydraulic Actuator Leakage Fault Detection using Extended Kalman Filter," International Journal of Fluid Power, 6(1), pp. 41-51.

[15] An, L., and Sepehri, N., 2006, "Hydraulic Actuator Leakage Quantification Scheme using Extended Kalman Filter and Sequential Test Method," American Control Conference, pp. 4424-4429.

[16] Skormin, V. A., and Apone, J., 1995, "On-Line Diagnostics of a Variable Displacement Pump of a Flightactuation System," IEEE Aerospace and Electronics Conference, 1, pp. 503-510.

[17] Karnopp, D., 1985, "Computer Simulation of Stick-Slip Friction in Mechanical Dynamic Systems," ASME Transactions Journal of Dynamic Systems, Measurement and Control, 107(1), pp. 100-103.

[18] Laval, L., M'Sirdi, N. K., and Cadiou, J. C., 1996, "H $_{infinity}$-Force Control of a Hydraulic Servo-Actuator with Environmental Uncertainties," Robotics and Automation, Proceedings of the IEEE , USA, 2, pp. 1566-1571.

[19] An, L., and Sepehri, N., 2004, "Leakage Fault Identification in a Hydraulic Positioning System Using Extended Kalman Filter," IEEE Proceedings of the American Control Conference (AAC), USA, 4, pp. 3088-3093.

[20] Niksefat, N., and Sepehri, N., 1999, "Robust Force Controller Design for an Electrohydraulic Actuatorbased on Nonlinear Model," Robotics and Automation, Proceedings of the IEEE International Conference, 1, pp. 200-206.

[21] Jerouane, M., Sepehri, N., Lamnabhi-Lagarrigue, F., 2004, "Design and Experimental Evaluation of Robust Variable Structure Control for Hydraulic Actuators," 5th Asian Control Conference, 3, pp. 1982- 1990.

[22] Iserman, R., 1984, "Process Fault Detection Based on Modeling and Estimation Methods," Automatica, 20(4), pp. 387-404.

[23] Isermann, R., 2005, "Model-Based Fault-Detection and Diagnosis - Status and Applications," Annual Reviews in Control, 29(1), pp. 71-85.

[24] Kalman, R. E., 1990, "Nine Lectures on Identification," Lecture Notes on Economics and Mathematical Systems, Springer Verlag.

[25] Simani, S., Fantuzzi, C., and Patton, R.J., 2003, "Model-Based Fault Diagnosis in Dynamic Systems Using Identification Techniques," Springer.

[26] Iserman, R., 1995, "Model Based Fault Detection and Diagnosis Method," Proceedings of the American Control Conference, 3, pp. 1603-1605.

[27] Venkatasubramanian, V., Rengaswamy, R., Yin, K., 2003, "A Review of Process Fault Detection and Diagnosis Part I: Quantitative Model-Based Methods," Computers and Chemical Engineering, 27(3), pp. 293-311.

[28] Venkatasubramanian, V., Rengaswamy, R., and Kavuri, S. N., 2003, "A Review of Process Fault Detection and Diagnosis Part II: Qualitative Models and Search Strategies," Computers and Chemical Engineering, 27(3), pp. 313-326.

[29] Venkatasubramanian, V., Rengaswamy, R., Kavuri, S. N., 2003, "A Review of Process Fault Detection and Diagnosis Part III: Process History Based Methods," Computers and Chemical Engineering, 27(3), pp. 327-346.

[30] Simani, S., Fantuzzi, C., Patton, R., 2004, "Model-Based and Data Driven Fault Diagnosis Methods with Applications to Process Monitoring," Springer.

[31] Frank, P. M., and Ding, X., 1994, "Frequency Domain Approach to Optimally Robust Residual Generation and Evaluation for Model-Based Fault Diagnosis," Automatica, 30(5), pp. 789-804.

[32] Chen, J., and Patton, R.J., 1999, "Robust Model-Based Fault Diagnosis for Dynamic Systems," Kluwer Academic Publishers, Boston/Dordrecht/London.

[33] Brogan, W.L., 1991, "Modern Control Theory," Prentice-Hall, Inc.

[34] Jiang, B., Staroswiecki, M., and Cocquempot, V., 2004, "Fault Diagnosis Based on Adaptive Observer for a Class of Non-Linear Systems with Unknown Parameters," International Journal of Control, 77(4), pp. 415-426.

[35] Kravaris, C., Sawoglidis, G., Kornaros, M., 2005, "Nonlinear Reduced-Order Observer Design for State And Disturbance Estimation," IEEE International Symposium on Intelligent Control and 13th Mediterranean Conference on Control and Automation, Cyprus, 2, pp. 1327-1332.

[36] Sfaihi, B., and Boubaker, O., 2004, "Full Order Observer Design for Linear Systems with Unknown Inputs," IEEE International Conference on Industrial Technology, Tunisia, 3, pp. 1233-1238.

[37] Arteaga, M. A., 2001, "Robust Control of Robots by using a Linear Observer," IEEE/ASME International Conference on Advanced Intelligent Mechatronics, Italy, 1, pp. 571-576.

[38] Zweiri, Y. H., and Seneviratne, L. D., 2006, "Diesel Engine Indicated and Load Torque Estimation using a Non-Linear Observer," Proceedings of the Institution of Mechanical Engineers, Part D (Journal of Automobile Engineering), 220(6), pp. 775-785.

[39] Willsky, A. S., 1976, "A Survey of Design Methods for Failure Detection in Dynamic Systems," Automatica, 12(6), pp. 601-611.

[40] Li-Ping, H., Hong-Zhong, H., and Zuo, M. J., 2007, "Fault Tree Analysis Based on Fuzzy Logic," IEEE Annual Reliability and Maintainability Symposium, USA, pp. 77-82.

[41] Tartakovsky, D. M., 2007, "Probabilistic Risk Analysis in Subsurface Hydrology," Geophysical Research Letters, 34(5), L05404.

[42] Iri, M., Aoki, K., O'Shima, E., 1979, "An Algorithm for Diagnosis of System Failures in the Chemical Process," Computers and Chemical Engineering, 3(1), pp. 489-493.

[43] Vedam, H., and Venkatasubramanian, V., 1997, "Signed Digraph Based Multiple Fault Diagnosis," Computers & chemical engineering, Elsevier, Norway, 21, pp. 655-660.

[44] Han, C., Shih, R., and Lee, L., 1994, "Quantifying Signed Direct Graphs with the Fuzzy Set for Fault Diagnosis Resolution Improvement," Industrial & Engineering Chemistry Research, 33(8), pp. 1943-1954.

[45] Umeda, Y., Koike, Y., Sato, T., 1992, "Model-Based Diagnosis using Qualitative Physics," Journal of the Japan Society of Precision Engineering/Seimitsu Kogaku Kaishi, 58(4), pp. 720-726.

[46] Sacks, E., 1988, "Qualitative Analysis by Piecewise Linear Approximation," First Annual Workshop on Qualitative Physics, USA, 3, pp. 151-155.

[47] Kresta, J. V., MacGregor, J. F., and Marlin, T. E., 1991, "Multivariate Statistical Monitoring of Process Operating Performance," Canadian Journal of Chemical Engineering, 69(1), pp. 35-47.

[48] Qin, S. J., and Li, W., 1999, "Detection, Identification, and Reconstruction of Faulty Sensors with Maximized Sensitivity," American Institute of Chemical Engineers Journal, 45(9), pp. 1963-1976.

[49] Dong, D., and McAvoy, T. J., 1996, "Batch Tracking Via Nonlinear Principal Component Analysis," American Institute of Chemical Engineers Journal, 42(8), pp. 2199-2208.

[50] Venkatasubramanian, V., and Chan, K., 1989, "A Neural Network Methodology for Process Fault Diagnosis," American Institute of Chemical Engineers Journal, 35(12), pp. 1993-2002.

[51] Ungar, L. H., Powell, B. A., and Kamens, S. N., 1990, "Adaptive Networks for Fault Diagnosis and Process Control," Computers & Chemical Engineering, 14(4), pp. 561-572.

[52] Watanabe, K., Hirota, S., Hou, L., 1994, "Diagnosis of Multiple Simultaneous Fault Via Hierarchical Artificial Neural Networks," American Institute of Chemical Engineers Journal, 40(5), pp. 839-848.

[53] Farell, A. E., and Roat, S. D., 1994, "Framework for Enhancing Fault Diagnosis Capabilities of Artificial Neural Networks," Computers & Chemical Engineering, 18(7), pp. 613-635.

[54] Tsai, C., and Chang, C., 1995, "Dynamic Process Diagnosis Via Integrated Neural Networks," Computers & Chemical Engineering, 19, pp. 747-752.

[55] Wang, X., and He, Y., 2005, "Diagonal Recurrent Neural Network Based On-Line Stator Winding Turn Fault Detection for Induction Motors," IEEE 8th International Conference on Electrical Machines and Systems, USA, 3, pp. 2266-2269.

[56] Lee, I. S., Kim, J. T., Lee, J. W., 2003, "Model-Based Fault Detection and Isolation Method using ART2 Neural Network," International Journal of Intelligent Systems, 18(10), pp. 1087-1900.

[57] Tafreshi, R., Ahmadi, H., Sassani, F., 2005, "Malfunction Detection in Multi-Cylinder Engines using Wavelet Packet Dictionary," SAE Technical Papers.

[58] Wang, X. Z., Chen, B. H., Yang, S. H., 1999, "Application of Wavelets and Neural Networks to Diagnostic System Development, 2, an Integrated Framework and its Application," Computers & Chemical Engineering, 23(7), pp. 945-954.

[59] Chen, B. H., Wang, X. Z., and McGreavy, C., 1998, "On-line operational support system for faults diagnosis in process plants," European Symposium on Computer Aided Process Engineering - 8, Belgium, 22, pp. 973-976.

[60] Zadeh, L. A., 1965, "Fuzzy Sets," Information and Control, 8(3), pp. 338-353.

[61] Hakami, B., and Newborn, J., 1983, "Expert System in Heavy Industry: an Application of ICLX in a British Steel Corporation Works," International Computers Limited Technical Journal , 3(4), pp. 347-359.

[62] Stewart, R. M., 1985, "Expert Systems for Mechanical Fault Diagnosis," Proceedings of the International Automatic Testing Conference, USA, pp. 295-300.

[63] Ramesh, T. S., Davis, J. F., and Schwenzer, G. M., 1992, "Knowledge-Based Diagnostic Systems for Continuous Process Operations Based upon the Task Framework." Computers and Chemical Engineering, 16(2), pp. 109-127.

[64] Tarifa, E. E., and Scenna, N. J., 1997, "Fault Diagnosis, Direct Graphs, and Fuzzy Logic," Computers and Chemical Engineering, 21, pp. 649-654.

[65] Scenna, N. J., 2000, "Some Aspects of Fault Diagnosis in Batch Processes," Reliability Engineering & System Safety, 70(1), pp. 95-110.

[66] Leung, D., and Romagnoli, J., 2000, "Dynamic Probabilistic Model-Based Expert System for Fault Diagnosis," Computers and Chemical Engineering, 24(11), pp. 2473-2492.

[67] Ghodsi, R., and Sassani, F., 2002, "An Adaptive Fuzzy Algorithm for Cut Sequencing of Solid Wood in Furniture Component Production," IEEE International Symposium on Intelligent Control, pp. 246-251.

[68] Ghodsi, R., and Sassani, F., 2005, "Real-Time Optimum Sequencing of Wood Cutting Process," International Journal of Production Research, 43(6), pp. 1127-1141.

[69] Cheung, J. T. Y., and Stephanopoulos, G., 1990, "Representation of Process Trends. Part I. A Formal Representation Framework," Computers & Chemical Engineering, 14(4), pp. 495-510.

[70] Vedam, H., and Venkatasubramanian, V., 1997, "Wavelet Theory-Based Adaptive Trend Analysis System for Process Monitoring and Diagnosis," Part 1 of 6, Proceedings of the American Control Conference, USA, 1, pp. 309-313.

[71] Maurya, M. R., Rengaswamy, R., and Venkatasubramanian, V., 2005, "Fault Diagnosis by Qualitative Trend Analysis of the Principal Components," Chemical Engineering Research & Design, 83, pp. 1122-1132.

[72] Zarchan, P., and Musoff, H., 2005, "Fundamentals of Kalman Filtering: A Practical Approach," Aiaa.

[73] Dalle Molle, D. T., and Himmelblau, D. M., 1987, "Fault Detection in a Single-stage Evaporator via Parameter Estimation using the Kalman Filter," Industrial & Engineering Chemistry Research, 26(12), pp. 2482-2489.

[74] Bergman, S., and Astrom, K. J., 1983, " Fault Detection in Boiling Water Reactors by Noise Analysis." Proceedings of the Fifth Power Plant Dynamics, USA, 2, pp. 29.01-29.20.

[75] Tsuge, Y., Ikeda, K., Shibata, B., 1992, "Hierarchical Fault Diagnosis System utilizing the Signed Directed Graph and the Extended Kalman Filter," IFAC/IMACS Symposium on Fault Detection, Supervision and Safety for Technical Processes, USA, pp. 439-444.

[76] Pirmoradi, F., Sassani, F., and de Silva, C.W., 2008, “Health Monitoring of Mechatronic System", in Mechatronic Systems: Devices, Design, Control, Operation and Monitoring, Editor: C. W. de Silva, CRC Press.

[77] Julier, S. J., and Uhlmann, J. K., 1997, "A New Extension of the Kalman Filter to Nonlinear Systems," Signal Processing, Sensor Fusion, and Target Recognition VI, Society of Photo-Optical Instrumentation Engineers, USA, 3068, pp. 182-193.

[78] Julier, S. J., and Uhlmann, J. K., 2004, "Unscented Filtering and Nonlinear Estimation," Proceedings of the IEEE, 92(3) pp. 401-422.

[79] Julier, S. J., Uhlmann, J. K., and Durrant-Whyte, H. F., 1995, "A New Approach for Filtering Nonlinear Systems," Proceedings of American Control Conference - ACC'95, Anonymous American Autom Control Council, USA, 3, pp. 1628-1632.

[80] Simon, D., 2006, "Optimal State Estimation: Kalman, H Infinity, and Nonlinear Approaches," Wiley-Interscience.

[81] Julier, S. J., Uhlmann, J. K., and Durrant-Whyte, H. F., 2000, "A New Method for the Nonlinear Transformation of Means and Covariances in Filters and Estimators," IEEE Transactions on Automatic Control, 45(3), pp. 477-482.

[82] Wan, E., and van der Merwe, R., 2001, "The Unscented Kalman Filter," John Wiley & Sons.